

# VERY LOW-MASS STARS AND BROWN DWARFS IN UPPER SCORPIUS USING GAIA DR1: MASS FUNCTION, DISKS AND KINEMATICS

NEIL J. COOK,<sup>1,2</sup> ALEKS SCHOLZ,<sup>3</sup> AND RAY JAYAWARDHANA<sup>2</sup>

<sup>1</sup>*Institut de Recherche sur les Exoplanètes, Université de Montréal, Montréal, QC, Canada, H3T 1J4*

<sup>2</sup>*Faculty of Science, York University, 4700 Keele Street, Toronto, Canada, ON M3J 1P3*

<sup>3</sup>*SUPA, School of Physics & Astronomy, University of St. Andrews, North Haugh, St. Andrews, KY16 9SS, UK*

(Received September 11, 2017; Revised October 16, 2017; Accepted October 17, 2017)

Submitted to AJ

## ABSTRACT

Our understanding of the brown dwarf population in star forming regions is dependent on knowing distances and proper motions, and therefore will be improved through the *Gaia* space mission. In this paper, we select new samples of very low mass objects (VLMOs) in Upper Scorpius using UKIDSS colors and optimised proper motions calculated using Gaia DR1. The scatter in proper motions from VLMOs in Upper Scorpius is now (for the first time) dominated by the kinematic spread of the region itself, not by the positional uncertainties. With age and mass estimates updated using Gaia parallaxes for early type stars in the same region, we determine masses for all VLMOs. Our final most complete sample includes 453 VLMOs of which  $\sim 125$  are expected to be brown dwarfs. The cleanest sample is comprised of 131 VLMOs, with  $\sim 105$  brown dwarfs. We also compile a joint sample from the literature which includes 415 VLMOs, out of which 152 are likely brown dwarfs. The disc fraction among low-mass brown dwarfs ( $M < 0.05 M_{\odot}$ ) is substantially higher than in more massive objects, indicating that discs around low-mass brown dwarfs survive longer than in low-mass stars overall. The mass function for  $0.01 < M < 0.1 M_{\odot}$  is consistent with the Kroupa IMF. We investigate the possibility that some ‘proper motion outliers’ have undergone a dynamical ejection early in their evolution. Our analysis shows that the color-magnitude cuts used when selecting samples introduce strong bias into the population statistics due to varying level of contamination and completeness.

*Keywords:* brown dwarfs — stars: lowmass — stars: mass function — open clusters and associations:  
individual: Upper Sco

## 1. INTRODUCTION

Most newly formed stars have masses significantly lower than the Sun. The characteristic mass of star formation, the peak of the Initial Mass Function (IMF), is around  $0.2 M_{\odot}$ , almost independent of environment (Bonnell et al. 2007). The mass distribution of objects formed in young clusters extends far below the sub-stellar limit at  $0.08 M_{\odot}$  and into the planetary (fusion-less) mass domain at  $< 0.015 M_{\odot}$  (Luhman 2012; Scholz et al. 2012). In this very low mass (VLM) domain, a variety of formation channels might play a role, including turbulent fragmentation of clouds, dynamical ejections from multiple systems, or disc fragmentation (see Whitworth et al. 2007).

Very low mass object (VLMOs) are also viable host stars for exoplanet systems, as evidenced by discoveries of Earth-sized or -massed planets around mid M dwarfs (Berta-Thompson et al. 2015; Anglada-Escudé et al. 2016; Dittmann et al. 2017; Gillon et al. 2017). The ubiquity of these systems poses an interesting challenge for core accretion theories, as discs around young objects in this mass domain usually do not seem to have sufficient material to form these type of systems (Scholz et al. 2006; Testi et al. 2015; Pascucci et al. 2016), implying very rapid formation. VLMOs are also possible hosts of ultracool dwarfs with L, T, or Y spectral types (Bardalez Gagliuffi et al. 2013; Cook et al. 2016, 2017).

Identifying and characterizing the VLM population in star forming regions provides the observational constraints on star formation scenarios as well as the samples for in-situ studies of planet formation. Traditionally, the selection of VLM cluster members is based on cuts in color-magnitude and proper motion space, followed by spectroscopy to confirm (Luhman et al. 2003; Wilking et al. 2004; Scholz et al. 2012). So far, proper motion cuts were limited to a few nearby regions with space motions significantly offset from the Galactic background. The output from the astrometry mission *Gaia* is about to change that (Gaia Collaboration et al. 2016a,b). It is anticipated that the final *Gaia* data releases will provide the first large, uniform sample of parallaxes for young brown dwarfs in addition to sub-milliarcsecond precision in proper motions.

*Gaia* published its first data release in 2017 (Gaia Collaboration et al. 2016a,b, henceforth *Gaia* DR1). While *Gaia* DR1 does not yet provide *Gaia*-internal parallaxes and has not yet reached optimum astrometric precision, it can already be used for improving current selection methods for young VLMOs and to refine the resulting samples, as we demonstrate in this paper for the nearest OB association Upper Scorpius. Using the combined parallaxes from the *Tycho-Gaia Astrometric Solution* (TGAS) for bright young stars, the estimates for distances, age and spatial depth for nearby star forming regions can be solidified. With the help of the *Gaia* DR1 astrometry, the scatter in proper motions from VLMOs in Upper Scorpius is now (for the first time) dominated by the kinematic spread of the region itself, not by the positional uncertainties. For this particular region later data releases are unlikely to significantly improve the member selection from proper motions. Upper Scorpius is a region mostly free from reddening, therefore follow-up spectroscopy is not as essential here as in other star forming regions.

In this paper, we estimate distance, age and spatial depth from higher-mass Upper Scorpius members (Section 2). We establish new samples of VLM members of Upper Scorpius using photometry from the *United Kingdom Infrared Digital Sky Survey Galactic Clusters Survey* (UKIDSS/GCS, Lawrence et al. 2007, see Section 3), and optimized astrometry obtained by combining *Gaia* DR1 with other catalogs (Section 4). Using these new samples we estimate masses (Section 5.1), test the disc fraction as a function of mass (Section 5.2) and the mass function (Section 5.3). We also make a first attempt at tracking down kinematic outliers (Section 5.4), i.e. objects with proper motions significantly different from their nearby siblings, which could be those who experienced an early dynamical ejection from a disc. The paper is intended to pave the way for future studies of other star forming regions based on the next *Gaia* data releases.

For the purposes of this paper, we use the term VLMO for all objects with masses below  $\lesssim 0.2 M_{\odot}$ , including very low mass stars, brown dwarfs and planetary mass objects.

## 2. THE UPPER SCORPIUS ASSOCIATION WITH GAIA DR1

When deriving stellar properties for members of star forming regions, the main source of uncertainty are distance and age. *Gaia* DR1 does not provide parallaxes for very low mass members of Upper Scorpius – this is expected to be included in later data releases – but the TGAS catalog does contain parallaxes for a substantial sample of early-type stellar members. TGAS<sup>1</sup>, is a combination of the *Tycho-2* with the *Gaia* catalog, listing astrometric data for  $\sim 2.5$

<sup>1</sup> Documentation available from [https://gaia.esac.esa.int/documentation/GDR1/Data\\_processing/chap\\_cu3tyc/](https://gaia.esac.esa.int/documentation/GDR1/Data_processing/chap_cu3tyc/)

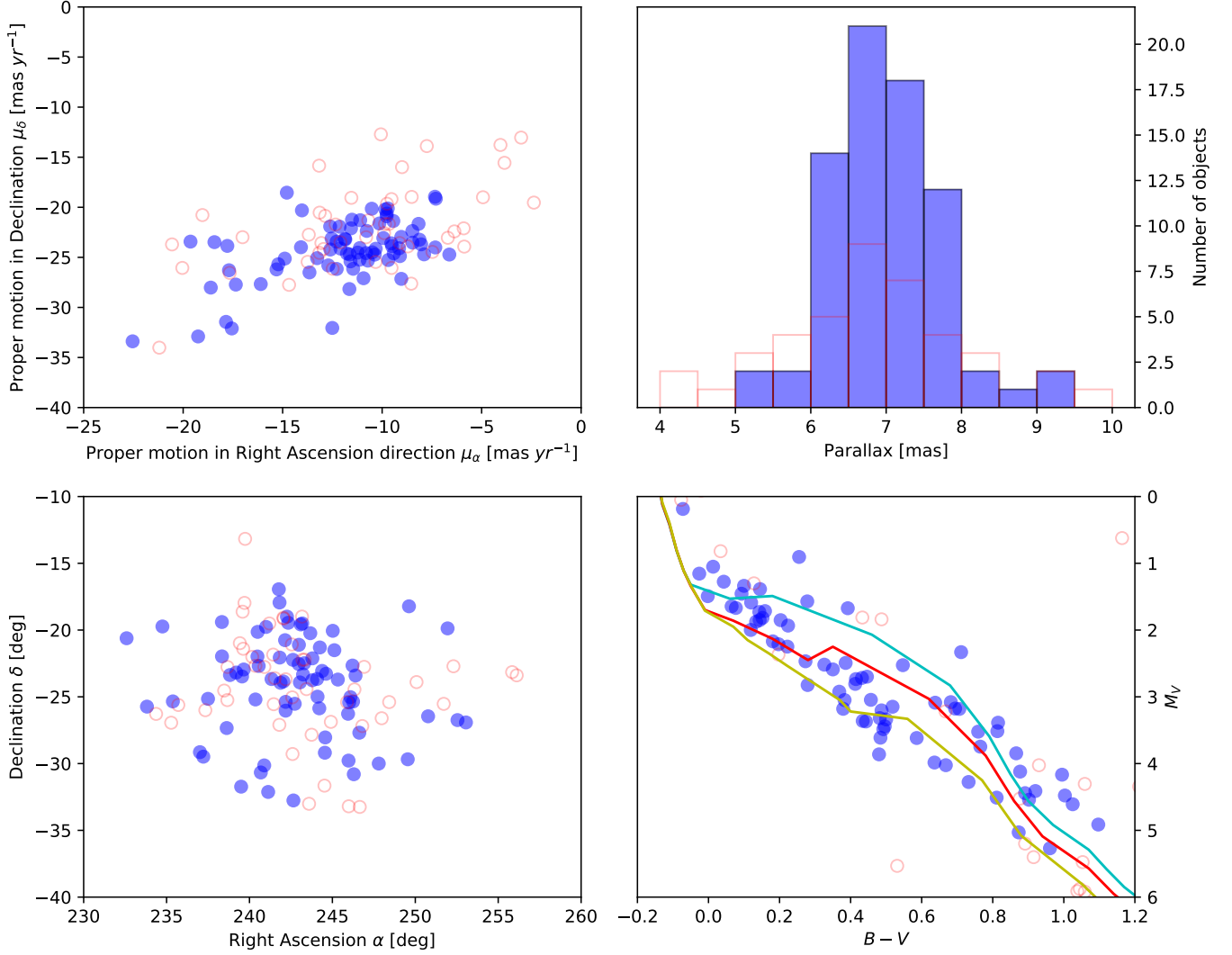


**Figure 1.** The 74 higher-mass members of Upper Scorpius used to determine distance, age and spatial depth for Upper Scorpius (in blue). The upper left panel shows their distribution in proper motion, the upper right panel shows their distance spread, the bottom left panel shows the distribution in space, and the lower right panel shows the color-magnitude diagram with 7, 10, and 15 *Myr* isochrones<sup>2</sup> (cyan, red, yellow) from Siess et al. (2000). Over-plotted in red are the rejected candidates.

million stars (Michalik et al. 2014; Gaia Collaboration et al. 2016a,b). In this section we aim to use this dataset to re-determine distance and age for Upper Scorpius.

We start with the sample of high-mass members of Upper Scorpius from de Zeeuw et al. (1999), selected as a moving group using Hipparcos astrometry. The mean Hipparcos distance in this sample is  $145 \pm 1$  pc. From the 120 members listed there, 85 have an entry in TGAS (with 1'' matching radius). From the catalog of primarily K-type members by Pecaute et al. (2012), we add 36 stars without Hipparcos, but with TGAS entry. To clean the sample, we remove objects with parallax error  $> 10\%$  (16 objects), without Tycho-2 photometry (4 objects) or magnitude error  $> 0.1$  mag (24 objects), and with implausible distances  $> 200$  pc (9 objects) leaving 74 objects (47 objects rejected in total, taking into account those rejected by multiple criteria).

Five of the rejected stars at distance  $> 200$  pc are classified as K-M giants in the Michigan Spectral Survey (Houk & Smith-Moore 1988), among them HIP83542, also rejected by Pecaute et al. (2012). In Figure 1, the cleaned sample has clusters around  $(-11.7, -24.2)$  mas yr<sup>-1</sup>, with standard deviation of 3 mas yr<sup>-1</sup>.

The cleaned sample of 74 stars have a median TGAS distance of 146.1 pc, and a mean TGAS distance of  $145 \pm 2$  pc. The median parallax error in this sample is 0.36 mas – this includes a systematic error of 0.14 mas, see Table 2 in

Arenou et al. (2017). The parallax error translates to a median distance error of 7.8 pc and a  $\sqrt{N}$  scaled error of  $\pm 0.9$  pc for the distance of the association. Thus, this provisional distance estimate from TGAS is within the error bars of the Hipparcos result. The parallax distribution (see Figure 1, upper right panel) has a standard deviation of 15.2 pc. Subtracting the errors in quadrature, this suggests a depth of the region along the line of sight of about  $\pm 13$  pc. For comparison, in the plane of the sky, the sample is contained within an area of 20 deg diameter in both RA and DEC, corresponding to 50 pc at the distance of Upper Scorpius.

From the cleaned sample, we produce a color-magnitude diagram (see Figure 1, lower right panel). The absolute magnitudes have been calculated using the individual TGAS distances for each star, eliminating the error caused by the depth of the region. Uncertainties in  $M_v$  and  $B - V$  are comparable to the size of the symbols for most objects. Variability is expected to have a minor effect on the position of the stars in the diagram for a region of this age. Without widespread accretion or discs (Luhman 2012), the only plausible source of variability is magnetic activity, which typically does not cause large amplitudes, even at this young age (Grankin et al. 2008). Therefore, the spread in the color-magnitude diagram likely corresponds to a real age spread in Upper Scorpius.

Over-plotted in Figure 1 are the 7, 10, and 15 *Myr* isochrones<sup>2</sup> (cyan, red, yellow) from Siess et al. (2000), using a metallicity of  $Z = 0.02$  (solar metallicity, Siess et al. 2000) and the Kenyon & Hartmann (1995) conversion table. These three isochrones bracket most of the sample for  $(B - V) < 0.8$ . For later-type objects the spread in the data points exceeds the model dispersion, partly due to increased photometric errors. Thus 7-15 *Myr* is a plausible minimum estimate for the age spread in this region. This is consistent with recent age studies for Upper Scorpius, see Pecaut & Mamajek (2016); Fang et al. (2017), but in conflict with earlier claims of  $5 \pm 2$  *Myr* by Preibisch et al. (2002). Note that we checked isochrones with non-solar metallicity and the differences were negligible for our purposes.

### 3. VERY LOW MASS OBJECTS IN UPPER SCORPIUS

Many previous works have studied the population of VLMOs in Upper Scorpius (e.g. Slesnick et al. 2008; Dawson et al. 2011; Lodieu et al. 2011; Luhman & Mamajek 2012; Dawson et al. 2013; Lodieu 2013; Lodieu et al. 2013; Dawson et al. 2014). Most use various color cuts to select potential VLMOs, and use proper motions (either calculated or obtained from large catalogs) to identify candidates moving in a similar way to known Upper Scorpius members. One of the main uncertainties of membership (when distance is unknown) is the uncertainties associated with the calculated proper motions. Thus more precise proper motions tend to lead to identifying a better sample of VLMOs in Upper Scorpius.

In this section we compile two samples, the first is a sample directly taken from the literature (and thus based on various colors cuts and slightly different selection criteria), henceforth the ‘L-sample’, the second is a large uniform sample, based on the initial color selection from Lodieu (2013), henceforth the ‘C-sample’.

#### 3.1. The L-sample

Although there are many surveys that study Upper Scorpius, we decided to choose those surveys that identify VLMO members using UKIDSS GCS (Lawrence et al. 2007) or similar (i.e. VISTA) photometry so that we had sub-samples that had Z, Y, J, H, K photometry (‘L-ZYJHK sample’); or had H and K photometry (‘L-HK only sample’). We combined data from Dawson et al. (2011), Lodieu et al. (2011), Dawson et al. (2013), Lodieu (2013), Lodieu et al. (2013), and Dawson et al. (2014) to obtain a sample of 789 unique objects, of which 493 were in the L-ZYJHK sample and 295 were in the L-HK only sample using photometry from both UKIDSS GCS DR10 (henceforth DR10) and the GCS Science verification release (henceforth SV; Dye et al. 2006). Tables 7 and 8 give the full detail on how many objects were in each source catalog.

#### 3.2. The C-sample

The data for the C-sample were obtained using the WFCAM Science Archive (WSA Hambly et al. 2008)<sup>3</sup> using SQL queries (see Appendix B). We followed the initial sampling used by Lodieu (2013), using identical bright saturation limits, limiting merged passband selection to 1'' and retaining only point-like, non-duplicated sources. We decided to also follow the sub-sample selection of Lodieu (2013), defining samples that had Z, Y, J, H, K photometry (‘C-ZYJHK sample’); or as having H and K photometry (‘C-HK only sample’). We obtained 2,653,897 sources for the C-ZYJHK

<sup>2</sup> <http://www.astro.ulb.ac.be/~siess/pmwiki/pmwiki.php/WWTools/Isochrones>

<sup>3</sup> WSA available on-line at <http://surveys.roe.ac.uk/wsa>.

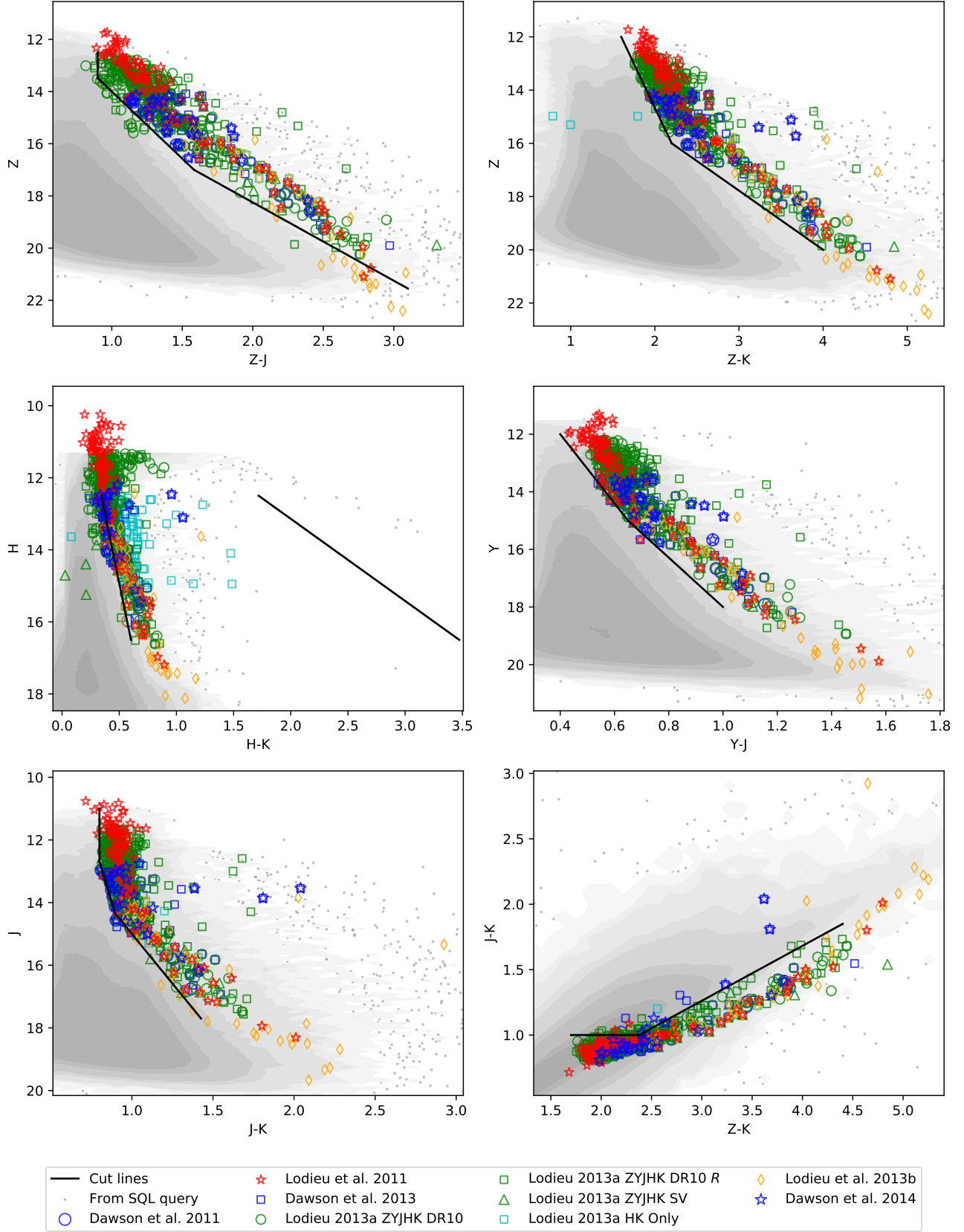


**Figure 2.** Color cuts applied to the samples obtained from the WSA. The gray contours show the data for the ‘C-ZYJHK DR10’ sample before the cuts were applied. Colored symbols show objects from the literature sample. The stars represent sources confirmed spectroscopically (Lodieu et al. 2011 or Dawson et al. 2014).

sample from DR10, 157,325 sources for the C-ZYJHK sample from SV, and 7,473,530 for the ‘HK sample’ of which 4,814,722 do not have Z, Y and J photometry (i.e. the C-HK only sample).

Following [Lodieu \(2013\)](#) we split the C-ZYJHK sample into a sub-sample affected by reddening and a sub-sample not affected by reddening (henceforth denoted as  $R$  for the reddened sample), and remove those objects with ‘HK extinction’ in the C-HK only sample (see table 1 from [Lodieu 2013](#)). The C-ZYJHK DR10 sample had 1,722,423 sources flagged as not affected by reddening and 931,474 flagged as being affected by reddening. The C-ZYJHK SV sample had no sources flagged as affected by reddening. The C-HK only sample had 3,652,715 that were not removed due to reddening.

To select VLMOs from the full samples we used the literature sample and the color cuts identified by [Lodieu \(2013\)](#). Our final color cuts are nearly identical to [Lodieu \(2013\)](#) except that we add an additional cut to  $H - K$ , this was in order to make sure our samples were not affected by the tail of the giant branch (See the  $H$  against  $H - K$  plot in Figure 2). The cuts are listed below.

$$\begin{aligned}
 \text{ZZJ cut} &= \begin{cases} Z - J > 0.90 & 12.50 < Z < 13.50 \\ Z < 5.14(Z - J) + 8.86 & 13.50 < Z < 17.00 \\ Z < 3.00(Z - J) + 12.25 & 17.00 < Z < 21.55 \end{cases} \\
 \text{HHK cut} &= \begin{cases} H < 15.38(H - K) + 7.23 & 12.50 < H < 16.50 \\ H > 2.28(H - K) + 8.58 & 12.50 < H < 16.50 \end{cases} \\
 \text{JJK cut} &= \begin{cases} J - K > 0.80 & 11.00 < J < 12.70 \\ J < 17.00(J - K) - 0.90 & 12.70 < J < 14.35 \\ J < 6.33(J - K) - 8.67 & 14.35 < J < 17.70 \end{cases} \\
 \text{ZZK cut} &= \begin{cases} Z < 6.67(Z - K) + 1.33 & 12.00 < Z < 16.00 \\ Z < 2.22(Z - K) + 11.11 & 16.00 < H < 20.00 \end{cases} \\
 \text{YYJ cut} &= \begin{cases} Y < 12.00(Y - J) + 7.20 & 12.00 < Y < 15.00 \\ Y < 8.57(Y - J) + 9.43 & 15.00 < Y < 18.00 \end{cases} \\
 \text{JKZK cut} &= \begin{cases} (J - K) < 1.00 & 1.70 < (Z - K) < 2.40 \\ (J - K) < 0.42(Z - K) & 2.40 < (Z - K) < 4.40 \end{cases}
 \end{aligned}$$

We decided to keep two different combinations of these cuts to see the effect they had on the final population selected, the first used all the above cuts (denoted by a HK) and the second used all the color cuts except the ‘HHK cut’.

Thus we have samples with ‘C-ZYJHK DR10’, ‘C-ZYJHK DR10  $R$ ’, ‘C-ZYJHK DR10 HK’, ‘C-ZYJHK DR10  $R$  HK’, ‘C-ZYJHK SV’, ‘C-ZYJHK SV HK’, and ‘C-HK only’ (where the ‘C’ distinguishes the sub-samples from the L-samples described in Section 3.1). The number of objects left after the color cuts are shown in Table 1 and a full break down of numbers is presented in tables 7 and 8.

### 3.3. Discussion of sub-samples

In summary we have two samples, the L-sample, constructed directly from the literature and the C-sample, constructed from UKIDSS DR10 and SV SQL Queries and color cuts. The L-sample is split into a ‘ZYJHK’ sample (comprising of objects with Z, Y, J, H and K photometry) and the ‘HK only’ (comprising of those object with only H and K photometry), these are named the ‘L-ZYJHK’ and ‘L-HK only’ samples. The C-sample is also split into a ‘ZYJHK’ and the ‘HK only’ sample (with the same definition), split by the data origin (i.e. either UKIDSS GCS DR10 or UKIDSS GCS SV) and by whether we use the ‘HHK cut’ (‘HKcut’) and whether the area the objects resides is



**Table 1.** The results for the C-samples after the color cuts are applied.

Sample	Total before cuts	ZZJ	HHK	JJK	ZZK	YYJ	JKZK	Total after cuts
C-ZYJHK DR10	1,722,423	5,654	-	23,134	9,977	12,122	245,810	1,305
C-ZYJHK DR10 <i>R</i>	931,474	1,538	-	9,940	2,569	5,824	400,451	811
C-ZYJHK SV	157,325	135	-	887	143	206	29,723	86
C-ZYJHK DR10 HK	1,722,423	5,654	2,359	23,134	9,977	12,122	245,810	66
C-ZYJHK DR10 <i>R</i> HK	931,474	1,538	318	9,940	2,569	5,824	400,451	77
C-ZYJHK SV HK	157,325	135	71	887	143	206	29,723	33
C-HK only	3,652,715	-	1,526	-	-	-	-	1,526

**Table 2.** The definition of the samples

Sample	Sub-sample	From DR10	From SV	Has Z, Y, J, H, and K photometry	Flagged as affected by reddening	HK Cut used
l-sample	L-ZYJHK	-	-	✓	-	-
	L-HK only	-	-	×	-	-
c-sample	C-ZYJHK DR10 HK	✓	×	✓	×	✓
	C-ZYJHK DR10 <i>R</i> HK	✓	×	✓	✓	✓
	C-ZYJHK SV HK	×	✓	✓	×	✓
	C-ZYJHK DR10	✓	×	✓	×	×
	C-ZYJHK DR10 <i>R</i>	✓	×	✓	✓	×
	C-ZYJHK SV	×	✓	✓	×	×
	C-HK only	✓	×	×	×	✓

flagged as having reddening (*R*). We do this so we can analyze the affect different cuts have on our results. Table 2 describes these sample subsets and their differences.

Each of our sub-samples has specific properties due to the imposed selection criteria. The C-HK only sample is going to be the least well defined sample due to the lack of Z, Y and J photometry and therefore lack of all the color cuts except the HK cut. The *R* samples (i.e. C-ZYJHK DR10 *R* and C-ZYJHK DR10 *R* HK) are expected to be more contaminated due to the increased reddening those source experience (i.e. reddened objects will be scattered across the color cuts). The SV samples (i.e. C-ZYJHK SV and C-ZYJHK SV HK) rely on science verification photometry and will be less complete than the DR10 samples. The SV samples also cover a slightly different spatial location than the DR10 samples and thus may have slight differences in age (see the age gradient from figure 9 of Pecaut & Mamajek 2016). The L-sample consists of some higher mass objects (due to the lack of, for example, brightness cuts), however due to some of these objects being spectroscopically confirmed we do not further reduce the L-sample and use it for comparative purposes only.

Our C-samples are much improved over the previously existing L-sample (due to our use of the best available color cuts and the better proper motion cuts (see Section 4). The addition of the HK cut to the C-ZYJHK samples add a brightness cut which essentially acts as a mass cut ( $\lesssim 0.2 M_{\odot}$  see effects in Section 5.3 and 5.2). This cut has the effect of avoiding contamination from red giants at the bright end of the magnitude distribution. Therefore, the C-ZYJHK DR10 HK should be the least contaminated sample among our sub-samples, but also the most restrictive. On the other

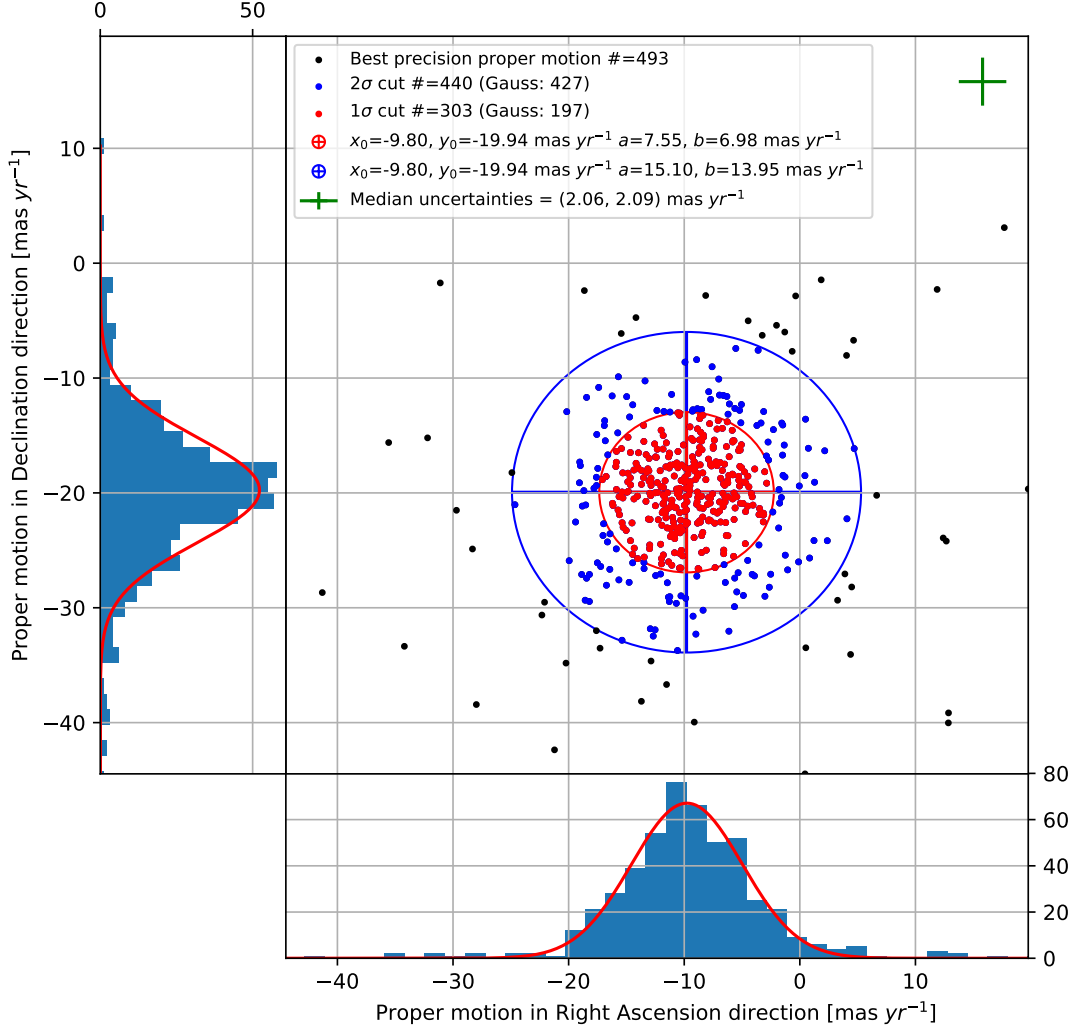


**Figure 3.** Proper motion vector diagram showing the one and two sigma ellipses used to define Upper Scorpius membership for the L-ZYJHK sample (for the best precision proper motions). The numbers of objects found were compared to a two-dimensional Gaussian distribution of equal center and covariance. Median uncertainties are shown in the upper right corner.

hand, the C-ZYJHK DR10 should be the most complete. Throughout this paper we do all analysis on all samples to check how much of an effect selection has on any results we obtain.

#### 4. PROPER MOTION ANALYSIS

As with many previous moving group membership surveys (e.g. Dawson et al. 2011, 2013; Lodieu 2013; Lodieu et al. 2013) we define Upper Scorpius membership as having a proper motion in both the Right Ascension and Declination directions consistent with that of Upper Scorpius. Since the release of the Gaia DR1 there have been new catalogs generated using the Gaia DR1 positions for objects without any Gaia proper motions (i.e. the Gaia DR1 secondary catalog of  $\sim 1.1$  billion sources, Gaia Collaboration et al. 2016b). Three of the largest proper motion catalogs currently using Gaia DR1 positions (and overlapping on-sky with Upper Scorpius) are the *Hot Stuff for One Year catalog*, (HSOY; containing  $\sim 583$  million stars Altmann et al. 2017), the *Gaia-PS1-SDSS proper motion catalog* (GPS1; containing  $\sim 350$  million stars, Tian et al. 2017), and the *US Naval Observatory CCD astrophot catalog 5* (UCAC5; containing  $\sim 107$  million stars, Zacharias et al. 2017). We cross-matched (selecting the closest source within a  $3''$  matching radius) all sub-samples (belonging to both the L-sample and the C-sample) with HSOY, GPS1 (also giving us access to the *Pan-STARRS1 proper motions*; PS1 Chambers 2011), UCAC5, as well as the PPMXL catalog (Roeser et al. 2010, containing  $\sim 900$  million sources), and the proper motions associated with each source from UKIDSS GCS DR10. From



**Table 3.** The result of the Upper Scorpius membership selection.

Sample	Total before cuts	Total after pm cuts
L-ZYJHK	453	415
L-HK	241	175
C-ZYJHK DR10	1,305	171
C-ZYJHK DR10 <i>R</i>	881	224
C-ZYJHK SV	68	58
C-ZYJHK DR10 HK	66	49
C-ZYJHK DR10 <i>R</i> HK	77	68
C-ZYJHK SV HK	17	14
C-HK only	1,519	346

these proper motions the most precise total proper motion was selected for each object (where total proper motion and associated uncertainty are defined in Equation 1).

$$\mu_{Total} = \sqrt{\mu_{\alpha}^2 + \mu_{\delta}^2} \quad \sigma_{\mu_{Total}} = \left| \frac{1}{\mu_{Total}} \right| \sqrt{(\sigma_{\mu_{\alpha}} \mu_{\alpha})^2 + (\sigma_{\mu_{\delta}} \mu_{\delta})^2} \quad (1)$$

where  $\mu_{\alpha}$  is the proper motion component in the Right Ascension direction ( $\cos(\delta)$ ) and  $\mu_{\delta}$  is the proper motion component in the Declination direction.

We decided to exclude PPMXL proper motions as no sources with only PPMXL proper motions had uncertainties better than  $\sim 10 \text{ mas yr}^{-1}$ . The stars that had a suitable proper motion measurement 716 out of 789 for the L-sample, all 2259 C-ZYJHK DR10 objects, 68 out of 86 C-ZYJHK SV objects, all 17 C-ZYJHK SV HK, 1,519 out of 1,526 C-HK only sample (see tables 7 and 8 for a full break down of numbers).

Our uncertainties in proper motion are sufficiently small that we do not need to select members based on a proper motion uncertainty circle (this is in contrast to previous studies where large uncertainties dominate the velocity dispersion of Upper Scorpius). However, since the proper motion of Upper Scorpius is very small, we decided to use the L-sample to define a two-sigma membership ellipse for Upper Scorpius (such that we avoid an overlap with  $(\mu_{\alpha}, \mu_{\delta}) = (0.0, 0.0) \text{ mas yr}^{-1}$ ). We compared the median and standard deviations for the L-ZYJHK, L-HK only and the combined sample. The L-ZYJHK sample was found to have a center of  $(\mu_{\alpha}, \mu_{\delta}) = (-9.80, -19.94) \text{ mas yr}^{-1}$ , with standard deviations of  $(\mu_{\alpha}, \mu_{\delta}) = (7.51, 6.96) \text{ mas yr}^{-1}$ . The L-HK only sample was found to have a center of  $(\mu_{\alpha}, \mu_{\delta}) = (-7.78, -18.39) \text{ mas yr}^{-1}$ , with standard deviations of  $(\mu_{\alpha}, \mu_{\delta}) = (7.82, 9.14) \text{ mas yr}^{-1}$ . The combined L-sample was found to have a center of  $(\mu_{\alpha}, \mu_{\delta}) = (-9.04, -19.46) \text{ mas yr}^{-1}$ , with standard deviations of  $(\mu_{\alpha}, \mu_{\delta}) = (7.88, 8.08) \text{ mas yr}^{-1}$ .

We thus chose to define candidate members of Upper Scorpius as those within an ellipse of center  $(\mu_{\alpha}, \mu_{\delta}) = (-9.80, -19.94)$  and x and y radii of  $(\mu_{\alpha}, \mu_{\delta}) = (15.10, 13.95) \text{ mas yr}^{-1}$  (defined from the L-ZYJHK distribution). This was then used to select members from the L-sample and C-sample. We keep 415/453 and 175/241 of those objects from the L-ZYJHK and L-HK only samples respectively. For the C-ZYJHK DR10 *R* sample we kept in 224/881 candidates, and 68/77 C-ZYJHK DR10 *R* HK candidates. For the C-ZYJHK sample we identified 171/1,305 candidates, and for the C-ZYJHK HK sample we kept 49/66 candidates. For the C-ZYJHK SV sample we identify 58/68 as Upper Scorpius candidates, and 14/17 for the C-ZYJHK SV HK sample. The C-HK only sample resulted in 346/1,519 candidates being identified. These numbers are summarized in Table 3 and tables 7 and 8 have a full break down of numbers. Figure 3 shows the L-ZYJHK sample used to selected candidates from both the L-samples and the C-samples.

The addition of a proper motion cut does confirm the characterization of the samples given in Section 3.3. Specifically, the C-HK sample without ZYJ photometry is heavily contaminated, as expected. The same applies to the C-ZYJHK DR10 and C-ZYJHK DR10 *R* samples. We expect most of the contamination in these samples to be at the bright magnitude end, i.e. at high masses in the VLM domain, because in this regime the population of young Upper Scorpius members is not well separated from the background population in color-magnitude diagrams. As mentioned above, the cleanest sample in our list are the ones with the HK cut, which removes objects at the bright end.

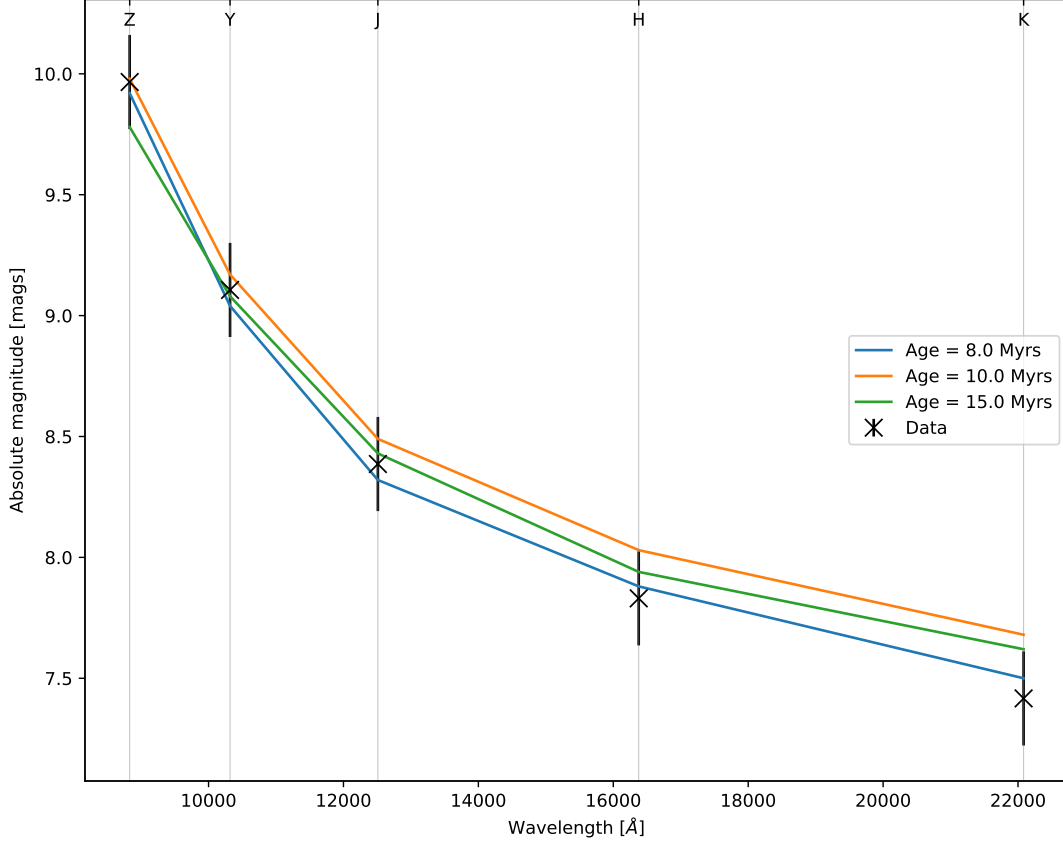


**Figure 4.** Example isochronal fit for L-sample object UGCS J161625.98-211222.9. Fit gives a mass of  $0.04^{+0.02}_{-0.01} M_{\odot}$ .

## 5. PROPERTIES OF VLMOS IN UPPER SCORPIUS

With an estimated age of 10 *Myr* (with a spread between 7 and 15 *Myr*) and assuming a distance of  $\sim 145$  pc (with a spread of  $\pm 13$  pc, Section 2) it is possible to estimate mass and luminosity by fitting the photometry to theoretical isochrones. We use the 8, 10 and 15 *Myr* Baraffe et al. (2015) isochrones (BHAC15) to give a lower, median and upper bound to each of our objects with UKIDSS Z, Y, J, H and K photometry (i.e. we only fit sources which have all five photometric magnitudes), we choose 8 *Myr* as the lower bound as the 7 *Myr* isochrone is not computed for BHAC15. In this section we describe the fitting process and use these, with *Wide-Field Infrared Survey Explorer* (WISE, Wright et al. 2010) data to infer a disc fraction, analyze the mass distributions and explore the proper motion distribution of our candidates.

### 5.1. Isochronal fitting

Using the 8, 10 and 15 *Myr* BHAC15 isochrones for UKIDSS we used chi-squared minimization (using the apparent UKIDSS magnitudes converted to absolute magnitudes using a distance of 146 pc, see Section 2) to select the best fit model for a lower, median and upper bounding model. The nature of the BHAC15 isochrones means for a given set of photometry (i.e. Z, Y, J, H and K) and age we get a mass estimate for each object (with an associated luminosity, effective temperature,  $T_{\text{eff}}$ , radius or surface gravity,  $\log(g)$  for each mass estimate).

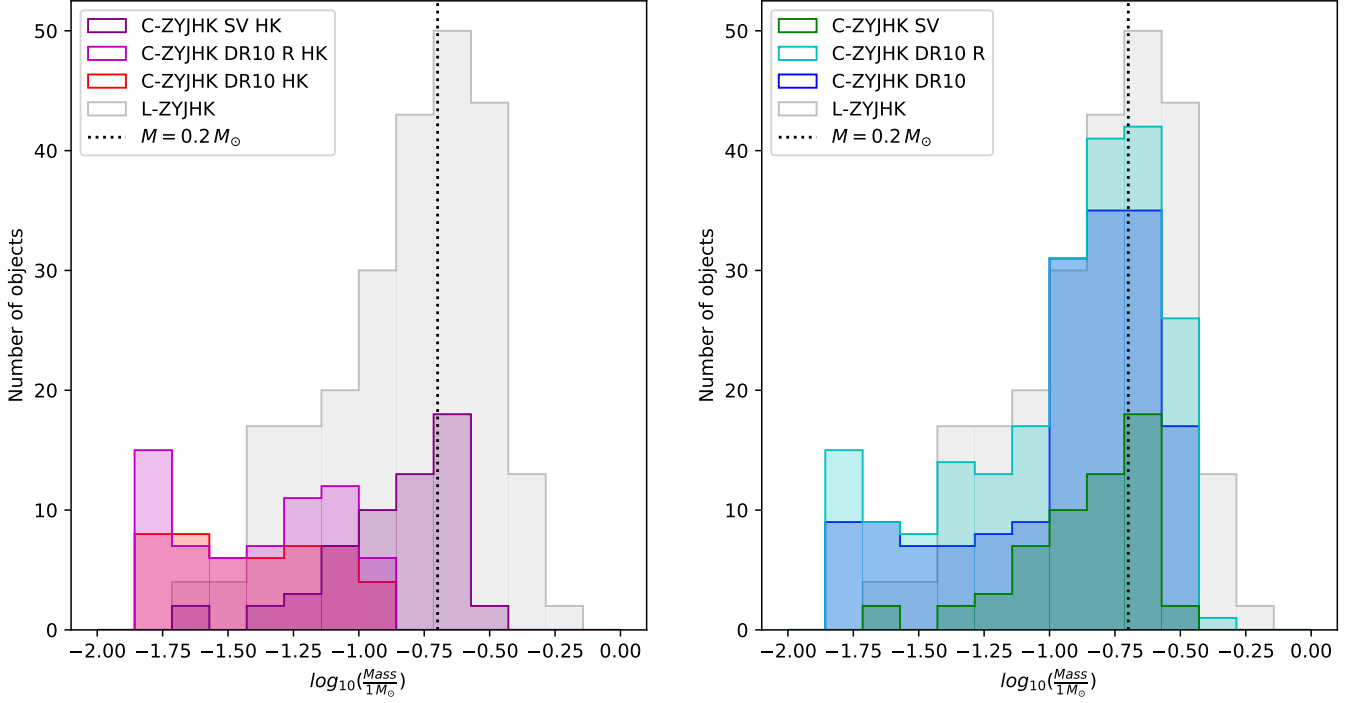


**Figure 5.** Log mass histogram for the C-sample using the HK cut (left) as compared to cases without (right). The HK cut effectively constrains the mass of the objects to  $\sim 0.2 M_{\odot}$  (black vertical line) whereas without the HK cut the masses extend to higher mass objects. Over-plotted, in both sub-plots for reference, is the L-sample (with no HK cut applied).

The mass estimate attached to each age (8, 10 and 15  $Myr$ ) were then combined, giving an expected value, an upper and a lower uncertainty (described in Equation 2).

$$\begin{aligned}
 \mathcal{M} &= (\mathcal{M}_{\text{median}})^{+\sigma_{\mathcal{M}_{\text{upper}}}}_{-\sigma_{\mathcal{M}_{\text{lower}}}} \\
 \mathcal{M}_{\text{median}} &= \text{median fit} \\
 \mathcal{M}_{\text{lower}} &= \text{lower fit} \\
 \mathcal{M}_{\text{upper}} &= \text{upper fit} \\
 \sigma_{\mathcal{M}_{\text{lower}}} &= \begin{cases} \mathcal{M}_{\text{upper}} - \mathcal{M}_{\text{median}} & \text{if } \mathcal{M}_{\text{lower}} = 0 \text{ and } \mathcal{M}_{\text{upper}} \neq 0 \\ \mathcal{M}_{\text{upper}} - \mathcal{M}_{\text{median}} & \text{if } \mathcal{M}_{\text{lower}} < 0 \text{ and } \mathcal{M}_{\text{upper}} < 0 \\ \mathcal{M}_{\text{median}} & \text{if } \mathcal{M}_{\text{lower}} = \mathcal{M}_{\text{upper}} = 0 \\ \mathcal{M}_{\text{median}} - \mathcal{M}_{\text{lower}} & \text{else-wise} \end{cases} \\
 \sigma_{\mathcal{M}_{\text{upper}}} &= \begin{cases} \mathcal{M}_{\text{median}} - \mathcal{M}_{\text{lower}} & \text{if } \mathcal{M}_{\text{lower}} = 0 \text{ and } \mathcal{M}_{\text{upper}} \neq 0 \\ \mathcal{M}_{\text{median}} - \mathcal{M}_{\text{lower}} & \text{if } \mathcal{M}_{\text{lower}} < 0 \text{ and } \mathcal{M}_{\text{upper}} < 0 \\ \mathcal{M}_{\text{median}} & \text{if } \mathcal{M}_{\text{lower}} = \mathcal{M}_{\text{upper}} = 0 \\ \mathcal{M}_{\text{upper}} - \mathcal{M}_{\text{median}} & \text{else-wise} \end{cases}
 \end{aligned} \tag{2}$$

where  $\mathcal{M}$  is the mass estimate associated with the best fit (lower, median and upper bounding) model. This gave us appropriate uncertainties for the estimated mass based on the spread in ages found for Upper Scorpius (Section 2). We do not interpolate between the models and these estimated masses assume that all objects have an age between 8 and 15  $Myr$  with a median of 10  $Myr$ . An example fit can be seen in Figure 4 for L-sample object UGCS J161625.98-211222.9.

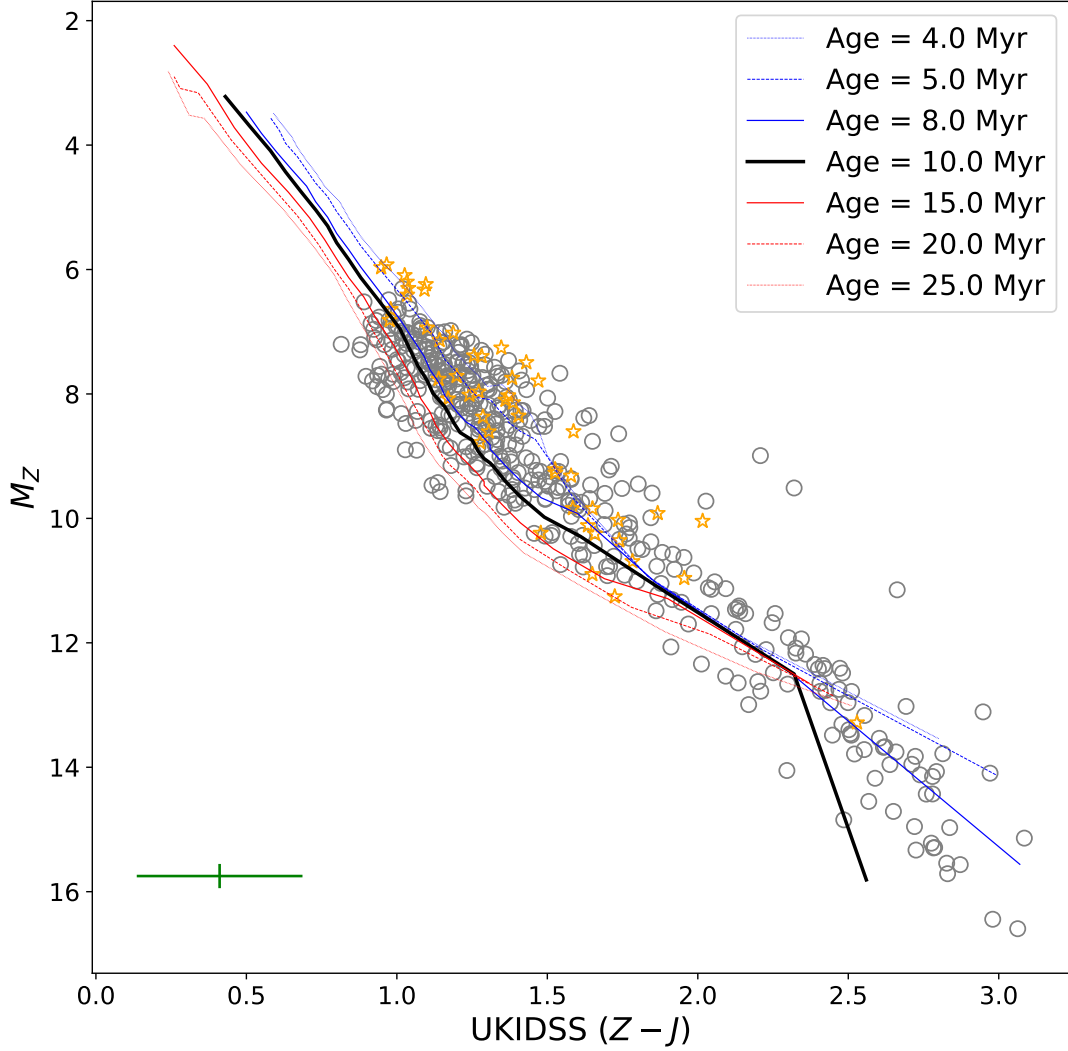


**Figure 6.** Absolute Z magnitude against  $(Z-J)$  color (Hertzsprung-Russell diagram) for the L-sample. Objects with discs are marked with an orange star. Median uncertainties are shown with the green cross. The distribution is consistent with an average age of 10 *Myr* and a spread from 8 to 15 *Myr*.

The estimated mass distributions for the C-sample using the HK cut as compared to cases without can be seen in Figure 5 (with the L-sample over-plotted in both cases for comparison). From Figure 5 the differences between the sub-samples becomes clear. The L-samples contain a significant number of higher-mass stars. The application of the HK cut (left panel compared to right panel) shows that this cut effectively removes objects of mass  $\lesssim 0.2 M_{\odot}$  and hence avoids contamination. The Hertzsprung-Russell diagram for the L-sample is shown in Figure 6. The distribution of colors seems consistent with a typical age of 10 *Myr*.

Defining brown dwarfs to have a mass less than  $0.075 M_{\odot}$  we calculated the number of our objects that are likely brown dwarfs (with the uncertainty coming from those that overlap in mass due to their mass estimate uncertainty). The L-ZYJHK sample was found to have  $152 \pm 38$  out of the 415 objects as likely brown dwarfs, the C-ZYJHK DR10 HK, C-ZYJHK DR10 *R* HK and C-ZYJHK SV HK samples were found to have  $42 \pm 11$ ,  $53 \pm 10$  and  $10 \pm 6$  respectively, and the C-ZYJHK DR10, C-ZYJHK DR10 *R* and C-ZYJHK SV samples were found to have  $48 \pm 13$ ,  $67 \pm 13$  and  $10 \pm 6$  respectively. These numbers are presented in Table 4. We note that the number of brown dwarfs are quite similar in the samples with and without the HK cut; in this mass domain the samples should avoid most contamination.

We were concerned that any objects with discs (see Section 5.2) may, due to their young age, have H and K photometry that is not well represented by one of the BHAC15 isochrones (i.e. there should be an additional component

**Table 4.** Numbers of possible brown dwarfs (Mass less than  $0.075 M_{\odot}$ ).

Sample	Total objects in sample	Likely brown dwarfs
L-ZYJHK	415	$152 \pm 38$
C-ZYJHK DR10 HK	49	$42 \pm 11$
C-ZYJHK DR10 <i>R</i> HK	68	$53 \pm 10$
C-ZYJHK SV HK	14	$10 \pm 6$
C-ZYJHK DR10	171	$48 \pm 13$
C-ZYJHK DR10 <i>R</i>	224	$67 \pm 13$
C-ZYJHK SV	58	$10 \pm 6$

added to the flux due to the presence of a disc). For this reason we also fitted the masses using only ZYJ and ZYJH and flagged any objects which were identified as having possible discs (from Section 5.2). This led to having three mass estimates for each object and thus we were able to see any differences due to ‘bad’ H and K photometry. After comparing objects with possible discs to those without discs no discernible difference was seen, thus the mass estimates were not affected by those objects having discs. Most objects had a maximum variation (due to using different sets of photometry) of  $0.01 M_{\odot}$  thus we decided to retain our mass estimates using all five bands.

Our chi-squared minimization does not take into account the uncertainties in magnitude (shown on Figure 4) and thus it does not take into account any uncertainty due to distance or spread in the association. Note that the spread in the association is significantly larger than the distance uncertainty on Upper Scorpius ( $145 \pm 2$  pc), i.e.  $\pm 13$  pc from Section 2, thus an additional uncertainty on the mass estimates will be introduced (this will be solved with later Gaia data releases giving distances to individual objects).

As a further sanity check for our mass estimates we compared our results to the Lodieu et al. (2011) and Dawson et al. (2014) samples which both have spectroscopically confirmed members of Upper Scorpius. We compare the spectral types from the literature to the mass estimates from the isochrones and compare the mass estimates from the literature to the mass estimates from the isochrone fits (see Figure 7). The figures show the expected trends and broad agreement, but there are also clear discrepancies. In the left panel of Figure 7 some objects (with very low masses) have surprisingly early spectral types, Dawson et al. (2014) concluded that some of these objects might be further away than the rest of the objects identified as being part of Upper Scorpius. For these objects our mass estimate will be underestimated. In the right panel of Figure 7 we find that our mass estimates are systematically higher (by  $\sim 1\sigma$ ) compared to Lodieu et al. (2011). That study derives masses by comparing bolometric magnitudes (derived from J-band) with NextGen/DUST models (Baraffe et al. 1998 and Chabrier et al. 2000 respectively), using a distance consistent with ours, but assume an age of 5 Myr (priv. comm. Lodieu 2017). Between 5 and 10 Myr, VLMOs drop in luminosity, i.e. assuming a younger age leads to lower mass estimates.

### 5.2. Disc fraction as a function of mass

Using the  $(W1 - W2)$  color excess cut and W3 excess cut from Dawson et al. (2013, shown in Equation 3) we were able to identify possible discs in our candidate members.

$$\begin{aligned}
 \text{W1W2 Disc} &= J < 60(W1 - W2) - 9 \\
 \text{W3 Disc} &= \text{SNR}_{W3} > 5 \text{ and } W3 < 10 \\
 \text{Disc} &= (\text{W1W2 Disc}) \text{ or } (\text{W3 Disc})
 \end{aligned} \tag{3}$$

For the L-ZYJHK sample we found 47/244 of the Upper Scorpius members with mass estimates had discs ( $19.3 \pm 2.5\%$ ). For the C-ZYJHK DR10 HK, C-ZYJHK DR10 *R* HK and C-ZYJHK SV HK samples we found 14/46, 11/64 and 4/14 respectively ( $30.4 \pm 6.8\%$ ,  $17.2 \pm 4.7\%$  and  $28.6 \pm 12.1\%$ ). For the C-ZYJHK DR10, C-ZYJHK DR10 *R* and C-ZYJHK SV samples we found 21/167, 29/217 and 17/57 respectively ( $12.6 \pm 2.6\%$ ,  $13.4 \pm 2.3\%$  and

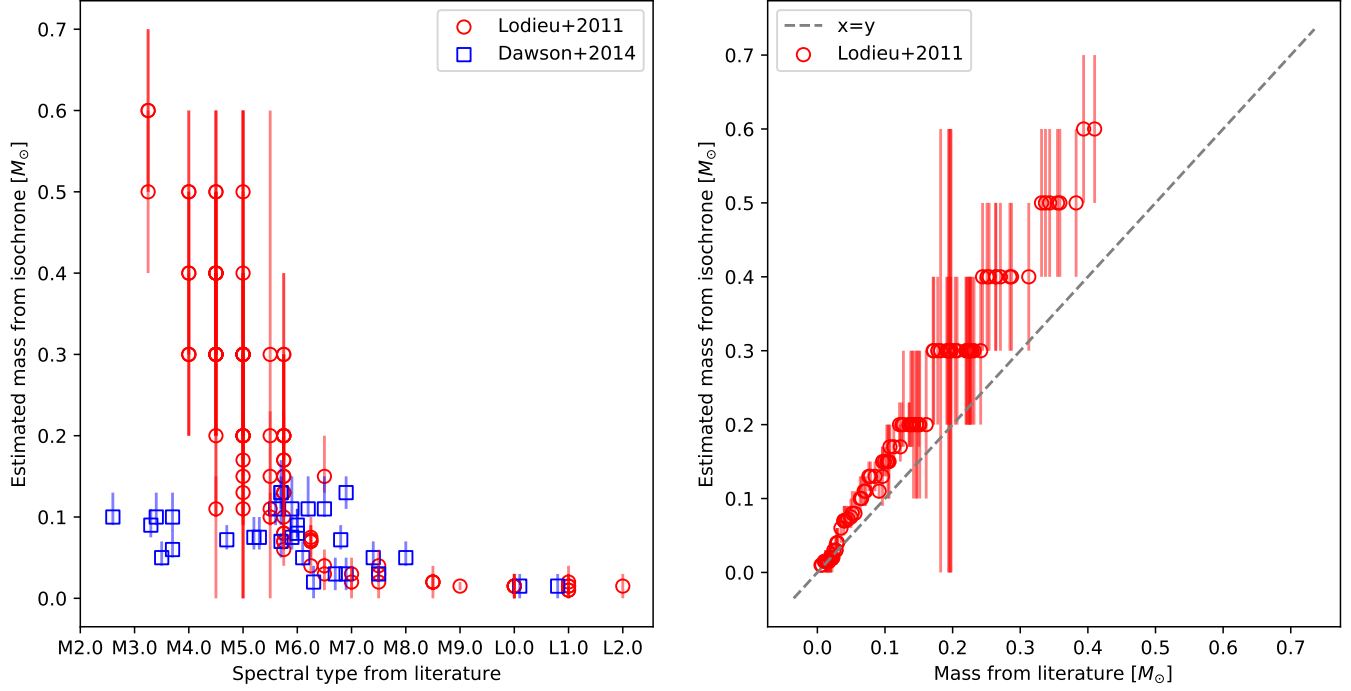


**Figure 7.** The comparison between our mass estimates from the isochrones to those objects in Upper Scorpius with spectral type and masses from the literature (members with spectra) from Lodieu et al. (2011) and Dawson et al. (2014).

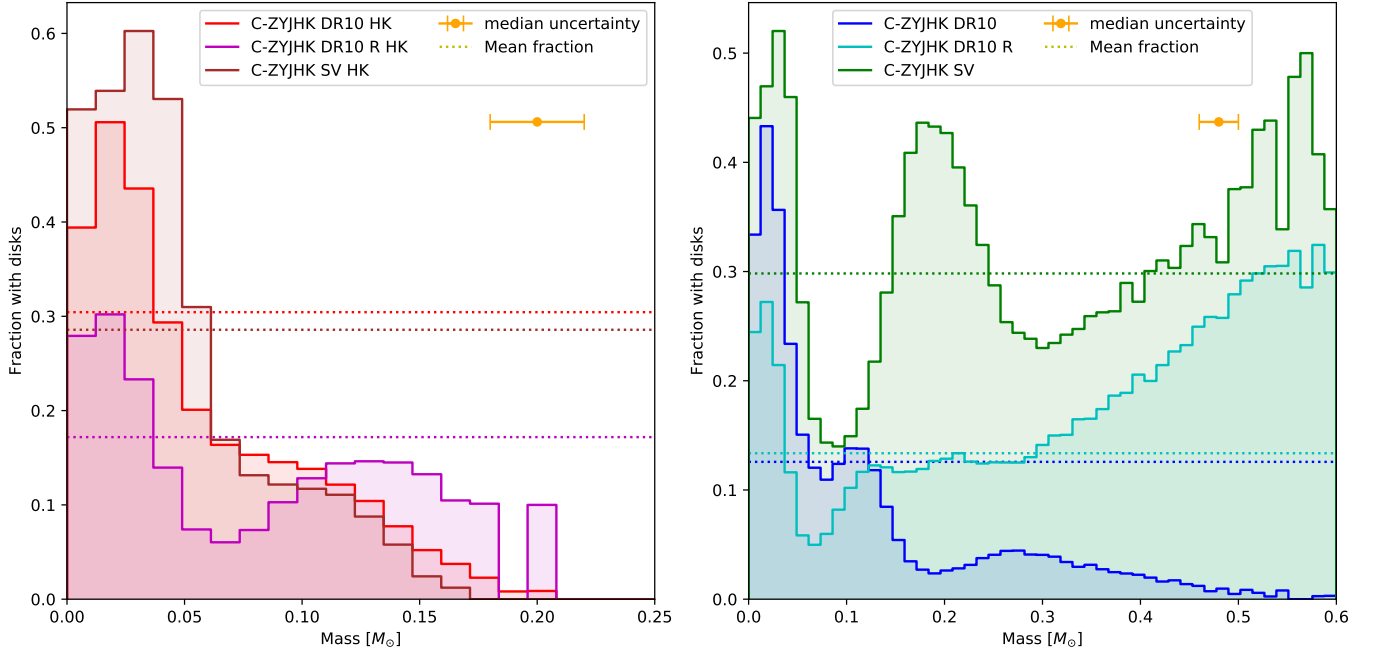


**Figure 8.** Disc fraction as a function of estimated mass (from isochrones). All samples were chosen to have 50 bins ranging from 0.0 to  $0.6 M_{\odot}$  (bin sizes were chosen to represent, approximately, the median uncertainty in mass estimates) and used 10,000 samples in our Monte-Carlo analysis (see Section 5.2) for those objects with mass estimates and with WISE photometry. Those flagged with discs were separated and fractions of object per mass bin were calculated. For those samples with the HK cut (left panel) we focus on the region from 0 –  $0.25 M_{\odot}$  level as no objects in the C-ZYJHK samples had larger masses.



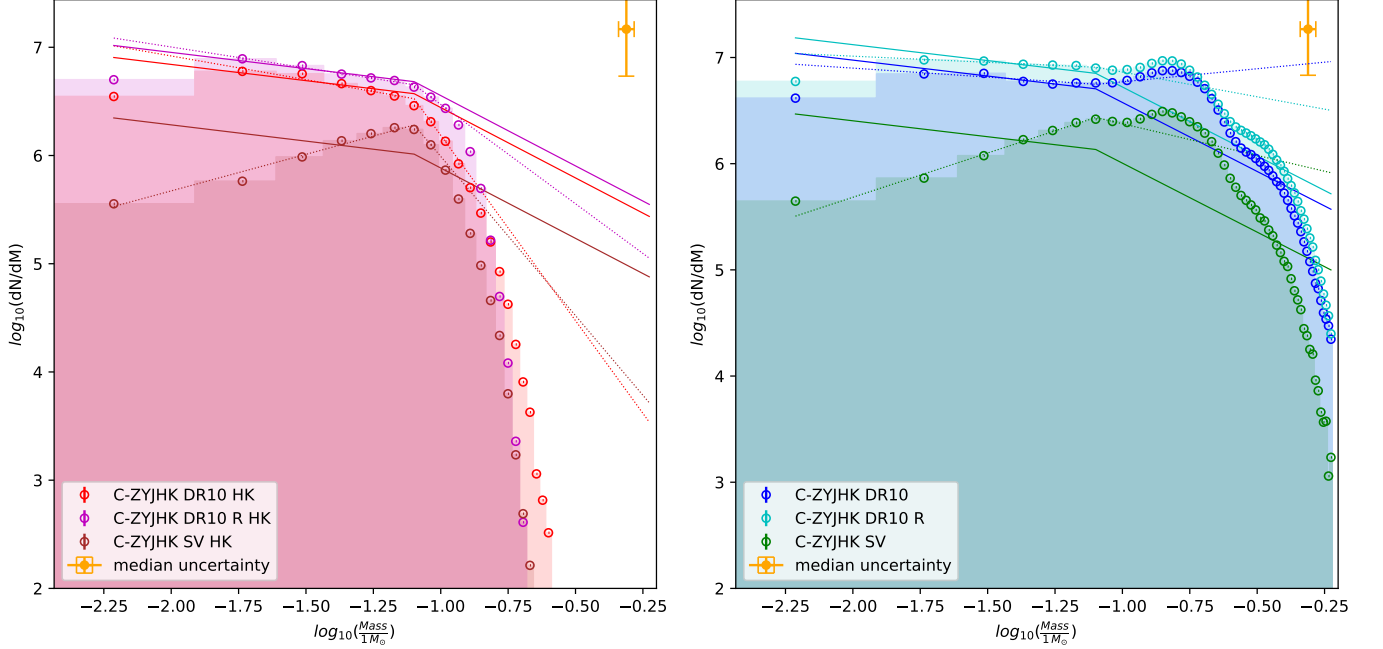


**Figure 9.** Mass functions (from isochrones). All samples were chosen to have 50 bins ranging from 0.0 to  $0.6 M_{\odot}$  (bin sizes were chosen to represent, approximately, the median uncertainty in mass estimates) and used 10,000 samples in our Monte-Carlo analysis (see Section 5.2) for those objects with mass estimates. The dashed lines show the best fits to a mass function ( $\alpha_1$  for  $0.08 < M < 0.5 M_{\odot}$ ,  $\alpha_2$  for  $M < 0.08 M_{\odot}$ ), where  $\alpha$  is allowed to vary and the solid lines show the Kroupa mass function ( $\alpha = 1.3$  for  $0.08 < M < 0.5 M_{\odot}$ ,  $\alpha = 0.3$  for  $M < 0.08 M_{\odot}$ ). All fits are scaled arbitrarily.

**Table 5.** The disc fractions found for the Upper Scorpius objects with WISE photometry.

Sample	Number of objects with discs	Number of objects in sample	Disc fraction
L-ZYJHK	47	244	$19.3 \pm 2.5\%$
C-ZYJHK DR10 HK	14	46	$30.4 \pm 6.8\%$
C-ZYJHK DR10 <i>R</i> HK	11	64	$17.2 \pm 4.7\%$
C-ZYJHK SV HK	4	14	$28.6 \pm 12.1\%$
C-ZYJHK DR10	21	167	$12.6 \pm 2.6\%$
C-ZYJHK DR10 <i>R</i>	29	217	$13.4 \pm 2.3\%$
C-ZYJHK SV	17	57	$29.8 \pm 6.1\%$

$29.8 \pm 6.1\%$ ), all fractions are presented in Table 5. Combined these give a weighted mean disc fraction of  $16.8 \pm 1.7\%$ . All uncertainties are calculated as one-sigma uncertainties assuming binomial statistics (see tables 7 and 8 for a full break down of numbers). This value is broadly consistent with previously published disc fractions for VLM stars and brown dwarfs in this region (Jayawardhana et al. 2003; Scholz et al. 2007).

We then used the mass estimates to plot disc fraction as a function of mass, where we account for uncertainties in the mass using a Monte-Carlo approach to draw samples from a Gaussian distribution for each object and then bin up the total samples for candidates, see Figure 8. For each object our Monte-Carlo approach draws a large number of samples from a Gaussian mass distribution (using the full-width-half-maximum as the larger of the lower and upper uncertainty band). Thus our binning process takes into account the uncertainties in mass estimates and shows the distribution as if there were a larger number of objects (note all disc fractions are carefully extrapolated in this process).

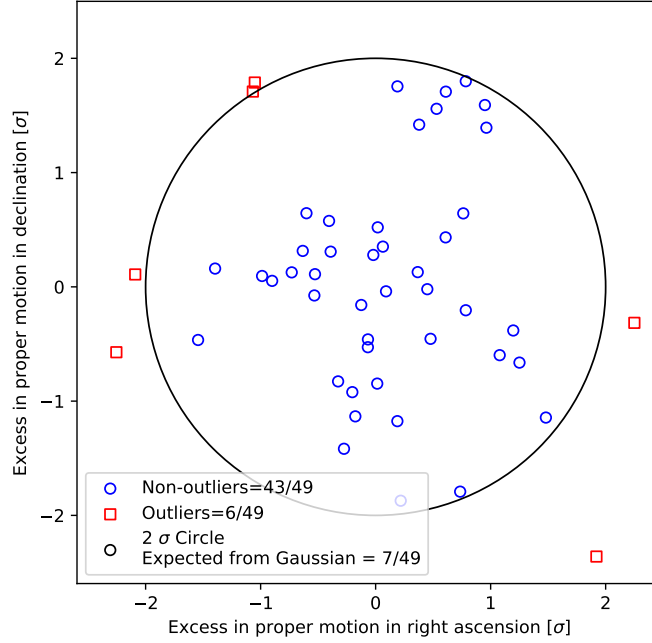


**Figure 10.** Proper motion excess diagrams for the C-ZYJHK DR10 HK sample. Excess is defined in Equation 4.

The disc fractions derived in that manner give two important insights. One is that the choice of the sample has a non-negligible effect on the outcome. This is particularly apparent from the right panel in Figure 8, which shows the sample without the HK cut. Based on our assessment of contamination of these samples (see Section 3.3 and Section 4 the disc fractions derived from these samples have to be treated with caution. Contamination by background red giants might increase the fraction of objects with infrared excess in these samples, while contamination by background dwarf stars would reduce it. The strong fluctuations of disc fraction as a function of mass seen in these samples will be caused primarily by the varying influence of these contaminating samples, rather than actual changes in the disc fraction of VLMOs in Upper Scorpius. Discrepancies on the brown dwarf disc fraction presented in the literature may to a large extent be caused by differences in sample selection.

Second, the clean samples with the HK cut do show that disc fractions within the sub-stellar domain increase with decreasing mass. This is seen in all three samples in the left panel of Figure 8. This trend was already stated in previous work, most notably by Luhman & Mamajek (2012). In our samples, the disc fraction for  $M < 0.05 M_{\odot}$  is about 2-3 times larger than at  $0.05 < M < 0.15 M_{\odot}$ . This is solid evidence for disc lifetimes significantly exceeding 10 Myr for low-mass brown dwarfs, confirming previous claims based on smaller samples (Riaz et al. 2009).

### 5.3. Mass function

Using the same MCMC process as in Section 5.2 we worked out the total number of objects in each mass bin. The mass function was then calculated using the total number of objects in each mass bin divided by the size of the mass bin. Uncertainties in number are assumed to be  $\sqrt{N}$ , and the uncertainty on  $dM$  is assumed to be the size of the mass bin. This means the uncertainty on  $dN/dM$  is dominated by the uncertainty on the mass estimates. In Figure 8 we plot the mass function with the median uncertainties shown in yellow and the mass functions from Kroupa (2001),  $\alpha = 1.3$  for  $0.08 < M < 0.5 M_{\odot}$ ,  $\alpha = 0.3$  for  $M < 0.08 M_{\odot}$ , scaled arbitrarily to match our number of objects. Note that  $N$ , and thus  $dN/dM$ , are 10,000 times higher than our samples due to the Monte-Carlo samples used.

From Figure 8 we can see that both the C-ZYJHK DR10 samples are a good match to the Kroupa IMF (between  $\sim 0.01$  and  $\sim 0.1 M_{\odot}$ , with best fits values of  $\alpha = 0.45$  and  $0.38$  for C-ZYJHK HK and C-ZYJHK R HK respectively). For the higher mass objects our brightness cuts impose mass cuts that are seen as the steep decrease in the number of objects with masses above  $0.1 M_{\odot}$ . At low masses (especially in the case of the UKIDSS science verification data) we see a gradual decrease in numbers of objects due to fainter objects being missed by UKIDSS (more so in the science verification data due to its preliminary shallow nature). Overall for the small area not affected by the brightness cuts

**Table 6.** The number of outliers (those with excess greater than 2 sigma) compared to the number of expected outliers from a Gaussian distribution (again beyond 2 sigma).

Sample	Total objects in sample	Non-outliers	Outliers	Expected Outliers from Gaussian
L-ZYJHK	415	347	68	57
C-ZYJHK DR10 HK	49	43	6	7
C-ZYJHK DR10 <i>R</i> HK	68	59	9	10
C-ZYJHK SV HK	14	10	4	2
C-ZYJHK DR10	171	134	37	22
C-ZYJHK DR10 <i>R</i>	224	187	37	30
C-ZYJHK SV	58	44	14	8

or the faintness limit our data is consistent with the Kroupa IMF. A value of  $\alpha \sim 0.4$  is also in line with previous determinations of the IMF in this region, e.g. , [Lodieu et al. \(2013\)](#) find  $\alpha = 0.45 \pm 0.11$ .

The right panel in Figure 8 which shows the samples without the HK cut again illustrates the effects of contamination on the mass function. In particular, there is a consistent ‘bump’ in the mass function just above  $0.1 M_{\odot}$ , which is most likely introduced by background objects. Echoing our previous comments, we would like to caution using this selection method for candidate members to derive population statistics for  $M > 0.1 M_{\odot}$ , unless comprehensive spectroscopic characterisation is carried out to confirm youth and membership.

#### 5.4. Proper motion outliers

In this subsection we explore the possibility that some of the VLMOs in Upper Scorpius have a dynamic history that deviates from the bulk of the population, for example, because they experienced an ejection in the early stages of their evolution, which might have stopped in-fall and constrained the mass. Ejections like that are part of a number of proposed formation scenarios for sub-stellar objects (e.g. [Whitworth et al. 2007](#)).

To test for this possibility, we compare the proper motion for each target compared to its ten nearest neighbors (nearest in Right Ascension and Declination). An excess in proper motion was calculated for each object and is defined in Equation 4.

$$\text{Excess } (\mu_{\alpha}) = \frac{(\mu_{\alpha})_{\text{Target}} - (\mu_{\alpha})_{\text{NN}}}{\sqrt{\sigma_{(\mu_{\alpha})_{\text{Target}}}^2 + \sigma_{(\mu_{\alpha})_{\text{NN}}}^2}} \quad (4)$$

$$\text{Excess } (\mu_{\delta}) = \frac{(\mu_{\delta})_{\text{Target}} - (\mu_{\delta})_{\text{NN}}}{\sqrt{\sigma_{(\mu_{\delta})_{\text{Target}}}^2 + \sigma_{(\mu_{\delta})_{\text{NN}}}^2}}$$

where  $(\mu_{\alpha,\delta})_{\text{NN}}$  is the median of the ten nearest neighbor objects proper motion in the Right Ascension/Declination direction, and  $\sigma_{(\mu_{\alpha,\delta})_{\text{NN}}}$  is the standard deviation of the ten nearest neighbor objects in the Right Ascension/Declination direction. Thus excess is in units of sigma, where a value of zero would equate to an object having a proper motion component exactly equivalent to that of it’s neighbors.

This allowed us to flag any candidates with excesses beyond 2 sigma (defined by a circle in proper motion space). For the L-ZYJHK and L-HK only sample we found 68/415 and 31/175 outlier in our Upper Scorpius candidates. For the C-ZYJHK DR10 HK, C-ZYJHK DR10 *R* HK and C-ZYJHK SV HK samples we found 6/49, 9/68 and 4/14 outliers in our Upper Scorpius candidates. For the C-ZYJHK DR10, C-ZYJHK DR10 *R* and C-ZYJHK SV samples we found 37/171, 37/224, 14/58 outliers in our Upper Scorpius candidates. Figure 10 shows the excess distribution in proper motion for two samples, with the 2 sigma circle drawn and outliers highlighted in red. The numbers are reported in Table 6.

Comparing the number of outliers with the outliers expected from a Gaussian distribution (last column in Table 6), there is currently no strong evidence for the presence of a population of brown dwarfs with kinematical properties

distinct from the bulk population in the same area. For samples without the HK cut, the number of outliers is again expected to be affected by contamination, as discussed throughout this paper. We note that a proper motion of 2 mas, currently the median uncertainty of our optimized proper motions, translates into a velocity in the plane of the sky of  $1.3 \text{ km s}^{-1}$ , which is comparable with the typical velocity dispersion found in radial velocity surveys of young brown dwarfs (Joergens 2006). Ejection velocities may in some cases be significantly beyond that level (Stamatellos & Whitworth 2009, Li et al. 2015), i.e. the lack of proper motion outliers already provides useful limits for formation scenarios. This topic is an area where we expect future data releases from Gaia to provide improved constraints.

## 6. CONCLUDING REMARKS

The *Gaia* mission is a powerful new tool in understanding star forming regions due to its new and future astrometry. For the first time regions such as Upper Scorpius are no longer limited by the uncertainty on proper motion (and with future Gaia data releases unknown distances). As such we show that both age and mass estimates can be vastly improved, giving insight into the initial mass function and through published photometry from WISE, the disc fractions of these populations. However, we caution that future inferences on populations (such as for example, but in no way limited to, mass functions and disc fraction) will be very dependent on the selection criteria used. It may be that rigorous selection (i.e. via full spectroscopic analysis) is required to really identify bona fide VLMOs and brown dwarfs from background objects and other contamination. This is especially valid for regions where reddening is important, but also applies, as shown in this paper, to regions free from extinction. Despite this we find that our mass functions (at least between  $0.01 < M < 0.1 M_{\odot}$ ) are consistent with the Kroupa IMF, that the disc fraction among low-mass brown dwarfs ( $M < 0.05 M_{\odot}$ ) is substantially higher than in more massive objects. We note that proper motions from Gaia will give us an opportunity to detect objects that were dynamically ejected early on. If done correctly, with future Gaia data and full spectroscopic follow-up the potential for nearby star forming regions to advance our knowledge of low-mass, very-low mass and planetary mass objects is extremely exciting.

## ACKNOWLEDGMENTS

We would like to thank the anonymous referee whose careful reading of this paper and excellent comments were very welcome. We would like to thank Ogyen Verhagen, former undergraduate student at the University in St Andrews, whose final year project results motivated parts of this work. This work was supported in part by NSERC grants to R.J. This work has made use of data from the European Space Agency (ESA) mission *Gaia* (<https://www.cosmos.esa.int/gaia>), processed by the *Gaia* Data Processing and Analysis Consortium (DPAC, <https://www.cosmos.esa.int/web/gaia/dpac/consortium>). Funding for the DPAC has been provided by national institutions, in particular the institutions participating in the *Gaia* Multilateral Agreement. Specifically we use Gaia DR1 data (Gaia Collaboration et al. 2016a, Gaia Collaboration et al. 2016b) with more details available from Arenou et al. (2017), Lindegren et al. (2016), van Leeuwen et al. (2017), Carrasco et al. (2016) and Evans et al. (2017). We make use of data products from WISE (Wright et al. 2010), which is a joint project of the UCLA, and the JPL/CIT, funded by NASA. The UKIDSS project is defined in Lawrence et al. (2007). UKIDSS uses the UKIRT Wide Field Camera (WFCAM; Casali et al. 2007). The photometric system is described in Hewett et al. (2006), and the calibration is described in Hodgkin et al. (2009). The pipeline processing and science archive are described in Hambly et al. (2008). We have used data from the DR10 data release and the science verification data, which are described in detail at <http://wsa.roe.ac.uk>. This work is based in part on services provided by the GAVO Data Center. This research has made use of the VizieR catalog access tool, CDS, Strasbourg, France (Ochsenbein et al. 2000). We acknowledge the use of data products from the HSOY catalog of Altmann et al. (2017), the GPS1 catalog of Tian et al. (2017), the UCAC5 catalog of Zacharias et al. (2017), the Pan-STARRS1 catalog of Chambers (2011) and the PPMXL database of Roeser et al. (2010). This research has made use of NASA’s Astrophysics Data System.

*Software:* ASTROPY (Astropy Collaboration et al. 2013), IPYTHON (Pérez & Granger 2007), MATPLOTLIB (Barrett et al. 2005; Hunter 2007), NUMPY (Jones et al. 2001; Oliphant 2007), SCIPY (Jones et al. 2001; Oliphant 2007), STILTS (Taylor 2006), TOPCAT (Taylor 2005), TQDM (da Costa-Luis et al. 2017)

## APPENDIX

### A. SQL QUERIES

#### A.1. The ZYJHK Sample

ZYJHK sample query (Private communications with N. Lodieu see Lodieu 2013). This query returned 2,653,897 sources from UKIDSS DR10 and 157,325 sources from the UKIDSS SV.

```

/* Start */
SELECT
    sourceID, ra, dec, zAperMag3, zAperMag3Err, yAperMag3, yAperMag3Err, jAperMag3, jAperMag3Err, hAperMag3
    , hAperMag3Err, k1AperMag3, k1AperMag3Err, muRa, muDec, sigMuRa, sigMuDec
FROM
    gcsSource
WHERE
    ra BETWEEN 232.0 AND 255.0
    AND dec BETWEEN -30.0 AND -15.0
    /* Bright saturation cut-offs */
    AND zaperMag3 > 11.3
    AND yaperMag3 > 11.5
    AND japerMag3 > 11.0
    AND haperMag3 > 11.30
    AND k1aperMag3 > 9.90
    /* Limit merged passband selection to 1 arcsec */
    AND zXi BETWEEN -1.0 AND +1.0
    AND yXi BETWEEN -1.0 AND +1.0
    AND jXi BETWEEN -1.0 AND +1.0
    AND hXi BETWEEN -1.0 AND +1.0
    AND k1Xi BETWEEN -1.0 AND +1.0
    AND zEta BETWEEN -1.0 AND +1.0
    AND yEta BETWEEN -1.0 AND +1.0
    AND jEta BETWEEN -1.0 AND +1.0
    AND hEta BETWEEN -1.0 AND +1.0
    AND k1Eta BETWEEN -1.0 AND +1.0
    AND (jppErrBits < 131072)
    AND (hppErrBits < 131072)
    AND (k1ppErrBits < 131072)
    /* Retain only point-like sources */
    AND (
        (
            ((zClass BETWEEN -2 AND -1) OR (zClassStat BETWEEN -3.0 AND +3.0))
            AND
            ((yClass BETWEEN -2 AND -1) OR (yClassStat BETWEEN -3.0 AND +3.0))
            AND
            ((jClass BETWEEN -2 AND -1) OR (jClassStat BETWEEN -3.0 AND +3.0))
            AND
            ((hClass BETWEEN -2 AND -1) OR (hClassStat BETWEEN -3.0 AND +3.0))
            AND
            ((k1Class BETWEEN -2 AND -1) OR (k1ClassStat BETWEEN -3.0 AND +3.0))
        )
        OR mergedClass BETWEEN -2 AND -1 OR mergedClassStat BETWEEN -3.0 AND +3.0
    )
    /* Retain only the best record when duplicated in an overlap region */
    AND (priOrSec = 0 OR priOrSec = frameSetID)
/* End */

```

#### A.2. The HK-only Sample

HK-only sample query (Private communications with N. Lodieu see Lodieu 2013). This query returned 7,473,530 sources from UKIDSS DR10.

```

/* Start */
SELECT
    sourceID, ra, dec, zAperMag3, zAperMag3Err, yAperMag3, yAperMag3Err, jAperMag3, jAperMag3Err, hAperMag3
    , hAperMag3Err, k1AperMag3, k1AperMag3Err, muRa, muDec, sigMuRa, sigMuDec
FROM
    gcsSource
WHERE
    ra BETWEEN 232.0 AND 255.0
    AND dec BETWEEN -30.0 AND -15.0
    /* Bright saturation cut-offs */

```

```

AND (zaperMag3 < -0.9e9 OR zaperMag3 > 11.3)
AND (yaperMag3 < -0.9e9 OR yaperMag3 > 11.5)
AND (japerMag3 < -0.9e9 OR japerMag3 > 11.0)
AND haperMag3 > 11.30
AND k_laperMag3 > 9.90
/* Limit merged passband selection to 1 arcsec */
AND (zXi BETWEEN -1.0 AND +1.0 OR zXi < -0.9e9)
AND (yXi BETWEEN -1.0 AND +1.0 OR yXi < -0.9e9)
AND (jXi BETWEEN -1.0 AND +1.0 OR jXi < -0.9e9)
AND hXi BETWEEN -1.0 AND +1.0
AND k_lXi BETWEEN -1.0 AND +1.0
AND (zEta BETWEEN -1.0 AND +1.0 OR zEta < -0.9e9)
AND (yEta BETWEEN -1.0 AND +1.0 OR yEta < -0.9e9)
AND (jEta BETWEEN -1.0 AND +1.0 OR jEta < -0.9e9)
AND hEta BETWEEN -1.0 AND +1.0
AND k_lEta BETWEEN -1.0 AND +1.0
AND (hppErrBits < 131072)
AND (k_lppErrBits < 131072)
/* Retain only point-like sources */
AND (
  (
    ((zClass BETWEEN -2 AND -1) OR (zClassStat BETWEEN -3.0 AND +3.0) OR (zClass = -9999))
    AND
    ((yClass BETWEEN -2 AND -1) OR (yClassStat BETWEEN -3.0 AND +3.0) OR (yClass = -9999))
    AND
    ((jClass BETWEEN -2 AND -1) OR (jClassStat BETWEEN -3.0 AND +3.0) OR (jClass = -9999))
    AND
    ((hClass BETWEEN -2 AND -1) OR (hClassStat BETWEEN -3.0 AND +3.0))
    AND
    ((k_lClass BETWEEN -2 AND -1) OR (k_lClassStat BETWEEN -3.0 AND +3.0))
  )
  OR mergedClass BETWEEN -2 AND -1 OR mergedClassStat BETWEEN -3.0 AND +3.0
)
/* Retain only the best record when duplicated in an overlap region */
AND (priOrSec = 0 OR priOrSec = frameSetID)
/* End */

```

## B. THE SAMPLES BY NUMBER

In tables 7 and 8 we show the source counts (i.e. the number of objects used from the original tables), the number of objects with proper motions in the HSOY, GPS1, UCAC, GCS, and PPMXL catalogs. We show the number of objects with a ‘most precise’ proper motion (in the ‘best pm’ column, i.e. the smallest uncertainty as chosen from the HSOY, GPS1, UCAC and GCS catalogs, see Section 4). We show the source counts for those object that have WISE photometry, have a disc as indicated by the Dawson cuts (‘W1W2 disc’, ‘W3 disc’ and the combination of the two ‘disc’ column, see Section 5.2). The ‘mass est.’ column describes whether we were able to find an isochronal model that fit the data (see Section 5.1). The ‘USco’ column gives the number in each which conforms to our selection criteria for an Upper Scorpius member (see Section 4) and the numbers of objects in Upper Scorpius with discs, with an isochronal mass estimate and with both a disc and an isochronal mass estimate are shown in the last three columns. Tables 9 and 10 show the column descriptions for the samples (tables available online in machine readable format).



**Table 7.** The source counts for the L-sample. For the L-sample numbers are also presented by original literature source catalog and how many sources are present in UKIDSS GCS DR10 and the UKIDSS GCS Science verification data. Tables available online in machine readable format.

Flag	Total	HSOY	GPS1	UCAC	GCS	PPMXL	best pm	WISE	W1W2	W3	Disc	Disc	mass est.	USco	USco+ disc	USco+ Wise+ mass est.	USco disc+ mass est.
In D11	28	12	21	0	28	23	28	12	1	0	1	0	28	20	1	8	1
In L11	91	63	77	36	91	83	91	62	6	14	17	14	91	88	16	59	16
In D13	108	53	80	1	108	86	108	52	11	5	11	5	108	104	11	49	11
In L13a ZYJHK	201	124	154	36	201	159	201	124	13	12	17	12	184	195	17	107	15
In L13a ZYJHK <i>R</i>	120	73	84	23	120	96	120	72	6	4	8	4	116	108	7	59	7
In L13a HK	250	180	191	29	250	225	250	176	32	18	32	18	9	184	30	2	0
In L13a ZYJHK SV	70	38	55	5	70	61	70	38	6	4	8	4	66	64	7	33	7
In L13b	25	9	7	0	25	13	25	9	4	2	4	2	25	22	3	7	3
In D14	30	14	24	0	30	25	30	14	4	3	4	3	30	23	4	9	4
In GCS SV	122	79	103	38	122	110	122	77	10	17	21	17	117	112	20	70	20
In GCS DR10	716	469	549	126	716	609	716	462	66	55	83	55	453	610	79	244	47
L-ZYJHK	453	276	345	93	453	372	453	273	33	36	49	36	453	415	47	244	47
L-HK only	241	178	187	29	241	220	241	174	32	18	32	18	0	175	30	0	0
Total	716	469	549	126	716	609	716	462	66	55	83	55	453	610	79	244	47

Notes:

- Source catalogs are as follows: D11 Dawson et al. (2011); L11 Lodieu et al. (2011); D13 Dawson et al. (2013); L13a Lodieu (2013); L13b Lodieu et al. (2013); D14 Dawson et al. (2014); and GCS Lawrence et al. (2007) - the UKIDSS GCS catalog.
- ZYJHK, *R*, and HK here is as in Lodieu (2013) not as in our definitions of ZYJHK, *R* or HK.
- SV denotes UKIDSS GCS science verification data, DR10 denotes data release 10 data.

**Table 8.** The source counts for the C-sample. Tables available online in machine readable format.

The C-sample with the HK cut applied.

Flag	Total	HSOY	GPS1	UCAC	GCS	PPMXL	WISE pm	best pm	W1W2	W3	Disc	mass est.	USco	USco+ disc	USco+ Wise+ mass est.	USco disc+ mass est.
C-ZYJHK DR10 HK	66	21	24	0	66	36	66	66	14	3	15	66	49	14	46	14
C-ZYJHK DR10 <i>R</i> HK	77	24	35	0	77	42	77	77	12	1	12	77	68	11	64	11
C-ZYJHK SV HK	17	12	14	0	17	15	17	17	5	0	5	17	14	4	14	4
C-ZYJHK total HK	160	57	73	0	160	93	160	160	31	4	32	160	131	29	124	29
C-HK only	1526	870	807	225	1526	1032	1519	1395	180	98	214	1526	346	88	331	88

The C-sample without the HK cut applied.

Flag	Total	HSOY	GPS1	UCAC	GCS	PPMXL	WISE pm	best pm	W1W2	W3	Disc	mass est.	USco	USco+ disc	USco+ Wise+ mass est.	USco disc+ mass est.
C-ZYJHK DR10	1305	1212	1177	1063	1305	1262	1305	1305	21	25	42	1305	171	21	167	21
C-ZYJHK DR10 <i>R</i>	811	688	728	546	811	752	811	797	24	19	33	811	224	29	217	29
C-ZYJHK SV	86	43	64	8	68	65	68	67	14	11	18	68	58	17	57	17
C-ZYJHK Total	2202	1943	1969	1617	2184	2079	2184	2145	59	55	93	2184	453	67	441	67

**Table 9.** Column descriptions for C-sample tables for C-ZYJHK DR10, C-ZYJHK DR10 *R*, C-ZYJHK SV, C-ZYJHK DR10 HK, C-ZYJHK DR10 *R* HK, and C-ZYJHK SV HK and tables are available online in machine readable format.

Column Name	Description	Unit	UCD
UID	Unique identifier (1)	...	meta.id;meta.main
RAdeg	Right Ascension in decimal degrees (J2000)	deg	pos.eq.ra;meta.main
DEdeg	Declination in decimal degrees (J2000)	deg	pos.eq.dec;meta.main
Zmag	UKIDSS Z magnitude	mag	phot.mag;em.IR
e_Zmag	uncertainty in Zmag	mag	stat.error;em.IR
Ymag	UKIDSS Y magnitude	mag	phot.mag;em.IR
e_Ymag	uncertainty in Ymag	mag	stat.error;em.IR
Jmag	UKIDSS J magnitude	mag	phot.mag;em.IR.J
e_Jmag	uncertainty in Jmag	mag	stat.error;em.IR.J
Hmag	UKIDSS H magnitude	mag	phot.mag;em.IR.H
e_Hmag	uncertainty in Hmag	mag	stat.error;em.IR.H
Kmag	K magnitude	mag	phot.mag;em.IR.K
e_Kmag	uncertainty in Kmag	mag	stat.error;em.IR.K
pm	Most precise proper motion	mas/yr	pos.pm
e_pm	Uncertainty in pm	mas/yr	stat.error;pos.pm
r_pm	Reference for pm (2)	...	meta.bib
pmRA	Most precise proper motion in RA	mas/yr	pos.pm;pos.eq.ra
e_pmRA	Uncertainty in pmRA	mas/yr	stat.error;pos.pm;pos.eq.ra
pmDE	Most precise proper motion in DE	mas/yr	pos.pm;pos.eq.dec
e_pmDE	Uncertainty in pmDE	mas/yr	stat.error;pos.pm;pos.eq.dec
WISE	Has WISE photometry (3)	...	code.meta
Disk	Flagged as having a disc (3) (4)	...	code.meta
MassFit	Best $\chi^2$ fit for mass	solMass	phys.mass
bMassFit	Lower uncertainty bound in MassFit	solMass	stat.error;phys.mass
BMassFit	Upper uncertainty bound in MassFit	solMass	stat.error;phys.mass
TeffFit	Best $\chi^2$ fit for effective temperature	K	phys.temperature.effective
bTeffFit	Lower uncertainty bound in TeffFit	K	stat.error;phys.temperature.effective
BTeffFit	Upper uncertainty bound in TeffFit	K	stat.error;phys.temperature.effective
LumFit	Best $\chi^2$ fit for luminosity	solLum	phys.luminosity
bLumFit	Lower uncertainty bound in LumFit	solLum	stat.error;phys.luminosity
BLumFit	Upper uncertainty bound in LumFit	solLum	stat.error;phys.luminosity
log(g)Fit	Best $\chi^2$ fit for surface gravity	[cm/s <sup>2</sup> ]	phys.gravity
blog(g)Fit	Lower uncertainty bound in log(g)Fit	[cm/s <sup>2</sup> ]	stat.error;phys.gravity
Blog(g)Fit	Upper uncertainty bound in log(g)Fit	[cm/s <sup>2</sup> ]	stat.error;phys.gravity
RadFit	Best $\chi^2$ fit for radius	solRad	phys.size.radius
bRadFit	Lower uncertainty bound in RadFit	solRad	stat.error;phys.size.radius
BRadFit	Upper uncertainty bound in RadFit	solRad	stat.error;phys.size.radius
chilow	Low fit $\chi^2$	...	stat.fit.chi2
chimid	Mid fit $\chi^2$	...	stat.fit.chi2
chihi	High fit $\chi^2$	...	stat.fit.chi2
WiseAndMass	Has WISE photometry and a mass estimate	...	meta.code
sigExpmRA	Sigma excess in pmRA	...	stat.value;pos.pm;pos.eq.ra
sigExpmDE	Sigma excess in pmDE	...	stat.value;pos.pm;pos.eq.dec
fnpnout	Not an outlier in pm; $2\sigma$ (3)	...	meta.code.member
fpmout	Is an outlier in pm; $2\sigma$ (3)	...	meta.code.member

Table 9 continued on next page

**Table 9** (*continued*)

Column Name	Description	Unit	UCD
<sup>1</sup> Of this merged detection as assigned by merge algorithm. ID is unique over entire WSA via program ID prefix.			
<sup>2</sup> hsoy = Hot Stuff for One Year (HSOY) catalog (Altmann et al. 2017); gps1 = Gaia-PS1-SDSS (GPS1) catalog (Tian et al. 2017); gcs = The UKIRT Infrared Deep Sky Survey (UKIDSS) catalog (Lawrence et al. 2007); and ucac = UCAC5: New Proper Motions Using Gaia DR1 catalog (Zacharias et al. 2017).			
<sup>3</sup> 1 = True, 2 = False			
<sup>4</sup> Dawson et al. (2013) WISE W1-W2 or WISE W3 disc.			

**Table 10.** Column descriptions for the L-sample tables (L-ZJYHK and L-HKonly). Tables available online in machine readable format.

Column Name	Description	Unit	UCD
UID	Unique ID from catalog creation	...	meta.id;meta.main
RAdeg	Right Ascension in decimal degrees (J2000)	deg	pos.eq.ra;meta.main
DEdeg	Declination in decimal degrees (J2000)	deg	pos.eq.dec;meta.main
Coord	Source of main coordinates	...	meta.bib
Cat	Catalog contained in (1)	...	meta.bib
Zmag	Most precise Z magnitude	mag	phot.mag;em.opt.Z
r_Zmag	Reference for Zmag (1)	...	meta.bib
e_Zmag	uncertainty in Zmag	mag	stat.error;em.opt.Z
Ymag	Most precise Y magnitude	mag	phot.mag;em.opt.Y
r_Ymag	Reference for Ymag (1)	...	meta.bib
e_Ymag	uncertainty in Ymag	mag	stat.error;em.opt.Y
Jmag	Most precise J magnitude	mag	phot.mag;em.IR.J
r_Jmag	Reference for Jmag (1)	...	meta.bib
e_Jmag	uncertainty in Jmag	mag	stat.error;phot.mag;em.IR.J
Hmag	Most precise H magnitude	mag	phot.mag;em.IR.H
r_Hmag	Reference for Hmag (1)	...	meta.bib
e_Hmag	uncertainty in Hmag	mag	stat.error;phot.mag;em.IR.H
Kmag	Most precise K magnitude	mag	phot.mag;em.IR.K
r_Kmag	Reference for Kmag (1)	...	meta.bib
e_Kmag	uncertainty in Kmag	mag	stat.error;phot.mag;em.IR.K
SpTCat	spt from source catalog	...	src.spType
r_SpTCat	Reference for SpTcat (1)	...	meta.bib
MassCat	Mass from source catalog	solMass	phys.mass
r_MassCat	Reference for MassCat (1)	...	meta.bib
fZYJHK	Flag whether source has valid ZYJHK photometry (2)	...	meta.code
fHKonly	Flag that source only has HK photometry (2)	...	meta.code
pm	Most precise proper motion	mas/yr	pos.pm
e_pm	Uncertainty in pm	mas/yr	stat.error;pos.pm
r_pm	Reference for pm (3)	...	meta.bib
pmRA	Most precise proper motion in RA	mas/yr	pos.pm;pos.eq.ra
e_pmRA	Uncertainty in pmRA	mas/yr	stat.error;pos.pm;pos.eq.ra
pmDE	Most precise proper motion in DE	mas/yr	pos.pm;pos.eq.dec
e_pmDE	Uncertainty in pmDE	mas/yr	stat.error;pos.pm;pos.eq.dec
MassFit	Best $\chi^2$ fit for mass	solMass	phys.mass
bMassFit	Lower uncertainty bound in MassFit	solMass	stat.error;phys.mass

*Table 10 continued on next page*

**Table 10** (*continued*)

Column Name	Description	Unit	UCD
BMassFit	Upper uncertainty bound in MassFit	solMass	stat.error;phys.mass
TeffFit	Best $\chi^2$ fit for effective temperature	K	phys.temperature.effective
bTeffFit	Lower uncertainty bound in TeffFit	K	stat.error;phys.temperature.effective
BTeffFit	Upper uncertainty bound in TeffFit	K	stat.error;phys.temperature.effective
LumFit	Best $\chi^2$ fit for luminosity	solLum	phys.luminosity
bLumFit	Lower uncertainty bound in LumFit	solLum	stat.error;phys.luminosity
BLumFit	Upper uncertainty bound in LumFit	solLum	stat.error;phys.luminosity
log(g)Fit	Best $\chi^2$ fit for surface gravity	[cm/s2]	phys.gravity
blog(g)Fit	Lower uncertainty bound in log(g)Fit	[cm/s2]	stat.error;phys.gravity
Blog(g)Fit	Upper uncertainty bound in log(g)Fit	[cm/s2]	stat.error;phys.gravity
RadFit	Best $\chi^2$ fit for radius	solRad	phys.size.radius
eRadFitL	Lower uncertainty bound in RadFit	solRad	stat.error;phys.size.radius
eRadFitU	Upper uncertainty bound in RadFit	solRad	stat.error;phys.size.radius
chilow	Low fit $\chi^2$	...	stat.fit.chi2
chimid	Mid fit $\chi^2$	...	stat.fit.chi2
chihi	High fit $\chi^2$	...	stat.fit.chi2
Disk	Flagged as having a disc (2) (4)	...	meta.code
WiseAndMass	Has WISE photometry and a mass estimate (2)	...	meta.code
sigExpmRA	Sigma excess in pmRA	...	stat.value;pos.pm;pos.eq.ra
sigExpmDE	Sigma excess in pmDE	...	stat.value;pos.pm;pos.eq.dec
fnotPMout	Not an outlier in pm; $2\sigma$ (2)	...	meta.code.member
fPMout	Is an outlier in pm; $2\sigma$ (2)	...	meta.code.member

<sup>1</sup> GCSSV = from UKIDSS Science verification (Lawrence et al. 2007); GCSDR10 = from UKIDSS DR10 (Lawrence et al. 2007); D11 = from Dawson et al. (2011)]; L11 = From Lodieu et al. (2011); D13 = from Dawson et al. (2013); L13a = from Lodieu (2013): L13a\_HK from HK sample, L13a\_ZYJHK\_SV from the ZYJHK UKIDSS Science verification sample, L13a\_ZYJHK\_red from the ZYJHK UKIDSS DR10 affected by reddening sample, L13a\_ZYJHK\_nored from the ZYJHK UKIDSS DR10 devoid of reddening sample; L13b = from Lodieu et al. (2013); D14 = from Dawson et al. (2014).

<sup>2</sup> 1 = True, 2 = False

<sup>3</sup> hsoy = Hot Stuff for One Year (HSOY) catalog (Altmann et al. 2017); gps1 = Gaia-PS1-SDSS (GPS1) catalog (Tian et al. 2017); gcs = The UKIRT Infrared Deep Sky Survey (UKIDSS) catalog (Lawrence et al. 2007); and ucac = UCAC5: New Proper Motions Using Gaia DR1 catalog (Zacharias et al. 2017).

<sup>4</sup> From isochrones (i.e have ZYJHKW1W2 photometry).

## REFERENCES

- Altmann, M., Roeser, S., Demleitner, M., Bastian, U., & Schilbach, E. 2017, *A&A*, 600, L4
- Anglada-Escudé, G., Amado, P. J., Barnes, J., et al. 2016, *Nature*, 536, 437
- Arenou, F., Luri, X. and Babusiaux, C., Fabricius, C., et al. 2017, *A&A*, 599, A50
- Astropy Collaboration, Robitaille, T. P., Tollerud, E. J., et al. 2013, *A&A*, 558, A33
- Baraffe, I., Chabrier, G., Allard, F., & Hauschildt, P. H. 1998, *A&A*, 337, 403
- Baraffe, I., Homeier, D., Allard, F., & Chabrier, G. 2015, *A&A*, 577, A42
- Bardalez Gagliuffi, D. C., Burgasser, A. J., & Gelino, C. R. 2013, *Mem. Soc. Astron. Italiana*, 84, 1041
- Barrett, P., Hunter, J., Miller, J. T., Hsu, J.-C., & Greenfield, P. 2005, in *Astronomical Society of the Pacific Conference Series*, Vol. 347, *Astronomical Data Analysis Software and Systems XIV*, ed. P. Shopbell, M. Britton, & R. Ebert, 91
- Berta-Thompson, Z. K., Irwin, J., Charbonneau, D., et al. 2015, *Nature*, 527, 204
- Bonnell, I. A., Larson, R. B., & Zinnecker, H. 2007, *Protostars and Planets V*, 149
- Carrasco, J. M., Evans, D. W., Montegriffo, P., et al. 2016, *A&A*, 595, A7
- Casali, M., Adamson, A., Alves de Oliveira, C., et al. 2007, *A&A*, 467, 777
- Chabrier, G., Baraffe, I., Allard, F., & Hauschildt, P. 2000, *ApJ*, 542, 464

- Chambers, K. C. 2011, in *Bulletin of the American Astronomical Society*, Vol. 43, American Astronomical Society Meeting Abstracts #218, 113.01
- Cook, N. J., Pinfield, D. J., Marocco, F., et al. 2016, *MNRAS*, 457, 2192
- . 2017, *MNRAS*, 467, 5001
- da Costa-Luis, C., L., S., Mary, H., et al. 2017, tqdm/tqdm: tqdm v4.19.1 stable, , , doi:10.5281/zenodo.1001783. <https://doi.org/10.5281/zenodo.1001783>
- Dawson, P., Scholz, A., & Ray, T. P. 2011, *MNRAS*, 418, 1231
- Dawson, P., Scholz, A., Ray, T. P., et al. 2013, *MNRAS*, 429, 903
- . 2014, *MNRAS*, 442, 1586
- de Zeeuw, P. T., Hoogerwerf, R., de Bruijne, J. H. J., Brown, A. G. A., & Blaauw, A. 1999, *AJ*, 117, 354
- Dittmann, J. A., Irwin, J. M., Charbonneau, D., et al. 2017, *Nature*, 544, 333
- Dye, S., Warren, S. J., Hambly, N. C., et al. 2006, *MNRAS*, 372, 1227
- Evans, D. W., Riello, M., De Angeli, F., et al. 2017, *A&A*, 600, A51
- Fang, Q., Herczeg, G. J., & Rizzuto, A. 2017, *ApJ*, 842, 123
- Gaia Collaboration, Prusti, T., de Bruijne, J. H. J., et al. 2016a, *A&A*, 595, A1
- Gaia Collaboration, Brown, A. G. A., Vallenari, A., et al. 2016b, *A&A*, 595, A2
- Gillon, M., Triaud, A. H. M. J., Demory, B.-O., et al. 2017, *Nature*, 542, 456
- Grankin, K. N., Bouvier, J., Herbst, W., & Melnikov, S. Y. 2008, *A&A*, 479, 827
- Hambly, N. C., Collins, R. S., Cross, N. J. G., et al. 2008, *MNRAS*, 384, 637
- Hewett, P. C., Warren, S. J., Leggett, S. K., & Hodgkin, S. T. 2006, *MNRAS*, 367, 454
- Hodgkin, S. T., Irwin, M. J., Hewett, P. C., & Warren, S. J. 2009, *MNRAS*, 394, 675
- Houk, N., & Smith-Moore, M. 1988, *Michigan Catalogue of Two-dimensional Spectral Types for the HD Stars*. Volume 4, Declinations -26.0 deg to -12.0 deg
- Hunter, J. D. 2007, *Computing in Science & Engineering*, 9, 90. <http://aip.scitation.org/doi/abs/10.1109/MCSE.2007.55>
- Jayawardhana, R., Ardila, D. R., Stelzer, B., & Haisch, Jr., K. E. 2003, *AJ*, 126, 1515
- Joergens, V. 2006, *A&A*, 446, 1165
- Jones, E., Oliphant, T., Peterson, P., & Others. 2001, *SciPy: Open source scientific tools for Python*, , . <http://www.scipy.org/>
- Kenyon, S. J., & Hartmann, L. 1995, *ApJS*, 101, 117
- Kroupa, P. 2001, *MNRAS*, 322, 231
- Lawrence, A., Warren, S. J., Almaini, O., et al. 2007, *MNRAS*, 379, 1599
- Li, Y., Kouwenhoven, M. B. N., Stamatellos, D., & Goodwin, S. P. 2015, *ApJ*, 805, 116
- Lindgren, L., Lammers, U., Bastian, U., et al. 2016, *A&A*, 595, A4
- Lodieu, N. 2013, *MNRAS*, 431, 3222
- Lodieu, N., Dobbie, P. D., Cross, N. J. G., et al. 2013, *MNRAS*, 435, 2474
- Lodieu, N., Dobbie, P. D., & Hambly, N. C. 2011, *A&A*, 527, A24
- Luhman, K. L. 2012, *ARA&A*, 50, 65
- Luhman, K. L., Briceño, C., Stauffer, J. R., et al. 2003, *ApJ*, 590, 348
- Luhman, K. L., & Mamajek, E. E. 2012, *ApJ*, 758, 31
- Michalik, D., Lindgren, L., Hobbs, D., & Lammers, U. 2014, *A&A*, 571, A85
- Ochsenbein, F., Bauer, P., & Marcout, J. 2000, *A&AS*, 143, 23
- Oliphant, T. E. 2007, *Computing in Science & Engineering*, 9, 10. <http://aip.scitation.org/doi/abs/10.1109/MCSE.2007.58>
- Pascucci, I., Testi, L., Herczeg, G. J., et al. 2016, *ApJ*, 831, 125
- Pecaut, M. J., & Mamajek, E. E. 2016, *MNRAS*, 461, 794
- Pecaut, M. J., Mamajek, E. E., & Bubar, E. J. 2012, *ApJ*, 746, 154
- Pérez, F., & Granger, B. E. 2007, *Computing in Science and Engineering*, 9, 21. <http://ipython.org>
- Preibisch, T., Brown, A. G. A., Bridges, T., Guenther, E., & Zinnecker, H. 2002, *AJ*, 124, 404
- Riaz, B., Lodieu, N., & Gizis, J. E. 2009, *ApJ*, 705, 1173
- Roeser, S., Demleitner, M., & Schilbach, E. 2010, *AJ*, 139, 2440
- Scholz, A., Jayawardhana, R., Muzic, K., et al. 2012, *ApJ*, 756, 24
- Scholz, A., Jayawardhana, R., & Wood, K. 2006, *ApJ*, 645, 1498
- Scholz, A., Jayawardhana, R., Wood, K., et al. 2007, *ApJ*, 660, 1517
- Siess, L., Dufour, E., & Forestini, M. 2000, *A&A*, 358, 593
- Slesnick, C. L., Hillenbrand, L. A., & Carpenter, J. M. 2008, *ApJ*, 688, 377
- Stamatellos, D., & Whitworth, A. P. 2009, *MNRAS*, 392, 413
- Taylor, M. B. 2005, in *Astronomical Society of the Pacific Conference Series*, Vol. 347, *Astronomical Data Analysis Software and Systems XIV*, ed. P. Shopbell, M. Britton, & R. Ebert, 29



- Taylor, M. B. 2006, in *Astronomical Society of the Pacific Conference Series*, Vol. 351, *Astronomical Data Analysis Software and Systems XV*, ed. C. Gabriel, C. Arviset, D. Ponz, & S. Enrique, 666
- Testi, L., Skemer, A., Henning, T., et al. 2015, *ApJL*, 812, L38
- Tian, H.-J., Gupta, P., Sesar, B., et al. 2017, *ArXiv e-prints*, arXiv:1703.06278
- van Leeuwen, F., Evans, D. W., De Angeli, F., et al. 2017, *A&A*, 599, A32
- Whitworth, A., Bate, M. R., Nordlund, Å., Reipurth, B., & Zinnecker, H. 2007, *Protostars and Planets V*, 459
- Wilking, B. A., Meyer, M. R., Greene, T. P., Mikhail, A., & Carlson, G. 2004, *AJ*, 127, 1131
- Wright, E. L., Eisenhardt, P. R. M., Mainzer, A. K., et al. 2010, *AJ*, 140, 1868
- Zacharias, N., Finch, C., & Frouard, J. 2017, *AJ*, 153, 166